Silicon (2023) 15:6147–6171
https://doi.org/10.1007/s12633-023-02498-0

RESEARCH

Effect of Silicon Carbide and Boron Carbide on Mechanical and Tribological Properties of Aluminium 7075 Composites for Automobile Applications

P. Bharathi[1] · T. Sampath Kumar[1]

Received: 17 March 2023 / Accepted: 29 April 2023 / Published online: 10 May 2023

Abstract
In the current study, aluminium 7075 were reinforced with different wt% (2 to 6) of silicon carbide (SiC) and aluminium 7075 hybrid composites reinforced with different wt% (2 to 6) of silicon carbide (SiC) with constant 2 wt% of boron carbide (B_4C) were fabricated using the Powder Metallurgy method. The microstructural study of sintered samples was performed using FESEM. This mechanical alloying process helped uniform distribution of SiC and B_4C particles throughout the aluminium matrix. Electron backscatter diffraction studies demonstrated that Al7075 + 6wt%SiC particles have a finer grain structure. Aluminium 7075 alloy composites analysed using XRD to confirm the peak phases. The higher hardness values were obtained for Al7075 + 6wt% SiC and Al7075 + 3wt%SiC + 2wt%B_4C composites as 195 HV and 161 HV respectively. The higher compressive strength values were obtained for Al7075 + 3wt%SiC and Al7075 + 2wt%SiC + 2wt%B_4C composites as 220 MPa and 175 MPa respectively. The density of hybrid composites had a considerable impact on the influence of SiC and B_4C particles. The surface nature of Al7075 + 2wt%SiC and Al7075 + 4wt%SiC + 2wt%SiC composites have obtained as hydrophilic and hydrophobic respectively. Based on the thermal conductivity measurement, it was found that the Al7075 + 6wt%SiC composite sample has obtained the thermal conductivity of 58.99 W/m.K. Furthermore, the investigation on wear studies showed the wear rate for Al7075 + 4wt%SiC and Al7075 + 6wt%SiC + 2wt%B_4C composite as smaller under the load of 10N. The Al7075 + 6wt%SiC and Al7075 + 2wt%SiC + 2wt%B_4C hybrid composites have a higher corrosion resistance than in a 3.5% than the other aluminium 7075 composite samples.

Keywords Al7075 · Silicon carbide · Boron carbide · Powder metallurgy · Microstructure · Mechanical Properties

1 Introduction

Over the past several years, there has been a change in research away from monolithic materials and toward composite materials in view of the growing need on a worldwide scale for materials known for low cost, high performance, good, acceptable quality. In the case of metal matrix composites (MMCs), Aluminium 7075 alloy are widely made and employed for structural applications in aerospace and automobile industries. This is mostly due to their high strength-to-weight ratios, low cost and strong resistance to wear [1, 2]. Aluminium alloys have been evaluated and found to be useful in various engineering fields, including functional and structural applications. This is due to the variations seen in the mechanical properties depending on the proportion of reinforcement and the chemical composition of the aluminium matrix. Aluminium 7075 alloys find use in a variety of applications, with the requirement of further reinforcement. They serve as matrix materials (continuous phase), with several properties through addition of desirable single and multiple reinforcement particulates (discrete constituent non-metallic ceramics), which include Gr, SiC, Al_2O_3, TiO_2, B_4C, fly ash and other similar materials [3, 4]. Development in hybrid materials is essential for support to the rapidly growing technologies used in a variety of applications. The focus of research interests have recently has been on the ability of aluminium matrix composites (AMCs) to change their physical properties (such as thermal expansion and density), their mechanical properties (such as hardness and compressive behaviour), their tribological properties, and other properties by changing the constituent or filler material phase. The next

✉ T. Sampath Kumar
sampathtpp@gmail.com

P. Bharathi
bharathi.p2019@vitstudent.ac.in

[1] School of Mechanical Engineering, Vellore Institute of Technology, Vellore 632014, Tamil Nadu, India

generation of aluminium matrix composites, also known as hybrid aluminium matrix composites, has the potential to meet the increasing demands of high-tech applications in the near and far future [5–7]. No research has been conducted on Al7075 in the development of hybrid composites using SiC + B_4C as reinforcements. Incorporation of Silicon Carbide (SiC) into metals creates hardness of increased levels, improved wear resistance and corrosion resistance. Aluminium and silicon carbide (SiC) are chemically compatible with each other, forming a strong bond inside the matrix. There are several benefits of the use of SiC as reinforcement due to its exceptional workability, ease of machining and low cost. SiC particles have high hardness, which is greater than that of aluminium. B_4C particles reinforced with aluminium composites for the improvement of its mechanical properties. B_4C is an excellent material, due to its high rigidity and hardness, and as its low density. Powder metallurgy is one of the rapidly developing areas in industrial applications due to benefits, that include great dimensional control and elimination of for secondary machining operations. Powder metallurgy is the process of manufacturing a component to a net form or near-net shape. Compared to other production techniques, the density of the components can be readily manipulated and controlled using the powder metallurgy approach. In the past, several studies have been conducted using powder metallurgy to include ceramic particles as reinforcements on pure aluminium [8–11]. Mulugundam Siva Surya et al. studied [12], Al7075/SiC composites with different SiC contents (5, 10, 15, 20, 25 and 30 Wt%) and their effective processing with the use of the powder metallurgy approach. The composite specimen with 15 wt% of SiC was seen having higher mechanical properties such as toughness, hardness and flexural strength than the other specimens. This is due to the uniform dispersal of the SiC particles throughout the matrix. Sattari et al. [13] investigated Al7075 reinforced SiC composites (4, 6, 8 vol.%) fabricated by powder metallurgy. In addition, the SEM showed increase in the number of voids with increase in the percentage of SiC in the materials. The duration of milling time and percentage of SiC in the composites had an effect on the compressive strength of the composite, due to reduction of particle size. The same general trend was seen with the hardness value and the strength value. After milling for 8 h for 8 vol% SiC, the composite developed a hardness of 79 HBN. Atrian et al. [14] investigated Al7075 composites reinforced SiC fabricated through powder metallurgy, and found enhancement of the mechanical properties. Increase in the amount of SiC nanoparticles in the compacted specimens resulted in improvements in the hardness, stiffness, and strength of the material. Halil karokoc et al. [15] made a study of the mechanical characteristics of Al6061 alloy reinforced with SiC (9,6,3,12 Wt%) and B_4C (9,6,3,12 Wt%) and manufactured using powder metallurgy, while Al6061-12 wt% B_4C had a higher hardness value of 76.0 HB. Microstructure analysis revealed the dispersal of particles throughout the composite that included 3 wt% of B_4C and 9 wt% of SiC. Anil Kumar G et al. [16] made experimental investigation of Aluminium 7075 alloy reinforced with B_4C (5,10 and 15 wt%) fabricated through powder metallurgy for the enhancement of the mechanical characteristics and wear behaviour. The findings of the compression strength test showed a rise in the final compressive strength with increase in the percentage of B_4C particles. The hardness test showed an increase in the hardness of the fabricated composite with an increase in the sintering temperature (from 450 °C to 600 °C) and an increase in the reinforcement content (from 0 to 15%). The wear tests revealed substantial enhancement of the wear resistance of the material with the addition of wt% B_4C. Despite this, there is only a few research done, in the determination of the effect of powder metallurgy route on the Aluminium 7075 composites that were reinforced with SiC. The novel aspect of this research includes in the production of hybrid Al7075 composite materials with better wear and mechanical characteristics through addition of SiC and B_4C particles. However, in this study, conventional reinforced (Al7075 + SiC) and double reinforced (Al7075 + SiC + B_4C) were manufactured with the use of powder metallurgy process. The primary objective of this research was to develop a hybrid composite of aluminium 7075 alloys as matrix material through incorporation of SiC and B_4C particles via powder metallurgy process. A study of the mechanical properties such as Field emission scanning electron microscopy (FESEM), X-ray diffraction (XRD), Electron back scattered diffraction (EBSD), Hardness, Compressive strength, Density, Porosity, Wettability, Thermal conductivity, Wear and Corrosion analysis was made and reported for Al7075 + SiC and Al7075 + SiC + B_4C composites.

2 Experimental Investigation

In this study, aluminium 7075 alloy was used as a matrix material. The aluminium 7075 matrix (99.0% purity) powder and the ceramic powders of SiC and B_4C were purchased from Pallav Chemicals and Solvents Pvt Ltd in Mumbai, India. The chemical composition of the aluminium 7075 alloys is shown in Table 1. SiC with a purity

Table 1 Chemical composition of Aluminium 7075 alloy

Element	Composition (wt%)
Zinc (Zn)	5.5
Magnesium (Mg)	2.1
Copper (Cu)	1.28
Ferrite (Fe)	0.30
Chromium (Cr)	0.4
Manganese (Mn)	0.016
Silicon (Si)	0.3
Titanium (Ti)	0.2
Aluminium (Al)	Remaining

Table 2 Powder properties of Al7075, SiC and B_4C particles

Characteristics	Al7075 alloy	Silicon carbide (SiC)	Boron Carbide (B_4C)
Density (g/cm^3)	2.81	3.21	2.52
Melting Point (^oC)	447	2730	2350
Morphology	Irregular	Angular	Angular

of 99.5% and particle size with less than 37 microns was used as the reinforcing material. Another reinforcement of B_4C powder (99.5% purity) with a particle size less than 63 microns was employed as reinforcement. Details of the properties of powdered Aluminium 7075 alloy, silicon carbide, and boron carbide are shown in Table 2. Figure 1(a) illustrates the morphological image and particle size distribution of Aluminium 7075 powder. Figure 1(b) shows the morphological image and particle size distribution of SiC powder. Figure 1(c) represents morphological image and particle size distribution of B_4C powder. The characteristics of the powder particle size distribution are shown in Table 3. The weights of reinforcements, ranging from 2 to 6 Wt%, were determined with the use of a precision weight scale made by Mettler Toledo. The matrix and the reinforcements were thoroughly mixed using mechanical stirring at a speed of 2000 rpm for the achievement of a powder combination with uniformity throughout. On the completion of the blending stage, compacting die was preheated to a temperature of up-to 350 °C for elimination of any leftover moisture and minimising the formation of air bubbles during the process of mixing the matrix and the reinforcements. This was done for preventing the formation of voids in the composite material. Aluminium 7075 alloy was employed as the matrix material, in the variations with wt% of silicon carbide (between 2 to 6 wt%) and constant wt% of boron carbide (2 wt%) used as reinforcements in the composites. Compacting was done using a hydraulic jack that was set to operate at a high pressure of 735 MPa. This helped preparation of samples with dimensions of 26 mm in diameter and 25 mm in height. Following the compact, the material was degassed for three hours at a temperature of 400 °C for removal of moisture, hydrogen, and oxygen. Finally, the acquired samples were subjected to a sintering process in a high-temperature furnace with an operating temperature of 550 °C for 3 h. Following the completion of the fabrication process, they were analysed for microstructure. The sintered composites of Al7075 + SiC and Al7075 + SiC + B_4C are shown in Fig. 2(a) and (b) respectively. Figure 3(a) depicts the micro-structure of Al7075 + 4wt%SiC composite. The elemental composition analysis of the Al7075 + 4wt%SiC composite is shown in Fig. 3(b). Figure 3(c) shows the microstructure of Al7075 + 4wt%SiC + 2wt%B_4C composite while Fig. 3(d) displays the Elemental composition analysis of Al7075 + 4wt%SiC + 2wt%B_4C composite. Field emission scanning electron microscopy (Thermo fisher FEI Quanta 250 FEG) was used for the analysis of microstructural morphology of the composites. The EBSD study of the Al7075 composites was carried out using Quanta 3D FEG. All the samples were ground using emery sheets with grades ranging from 80 to 1200 grit, and then they were polished using a diamond paste solution with 1 µm particle size. After being ground and polished, the samples of the Al7075 composites were subjected to further electro-polishing with a 20% perchloric acid and 80% ethanol solution for approximately 10 min by applying a voltage of 20 V. X-ray diffraction analysis (Bruker D8

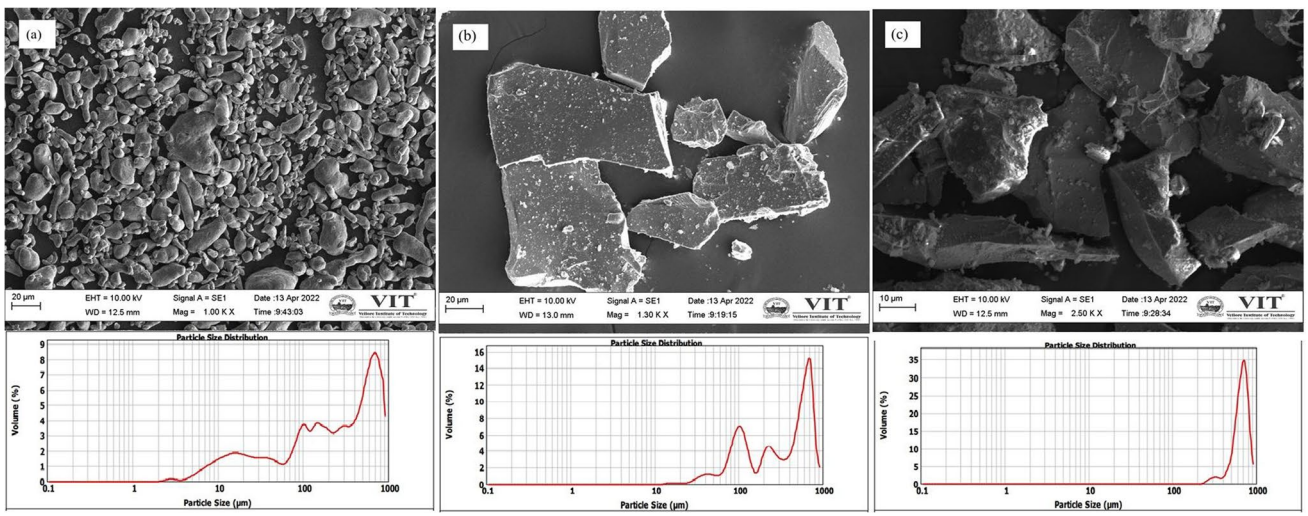

Fig. 1 Powder Particle morphology and particle size distribution **a** Al7075 **b** SiC **c** B_4C

Table 3 Characteristic values for the particle size distribution of different powders

Powder name	d_{10} (μm)	d_{50} (μm)	d_{90} (μm)	Span	Specific Surface Area (m^2/g)
Al7075	15.879	227.089	754.661	3.253	0.12
SiC	80.702	371.022	736.605	1.768	0.0347
B_4C	493.051	676.361	816.104	0.478	0.00958

diffractometer) was used for carrying out a phase identification study for composites. A Vickers hardness testing machine (Model: Matsuzawa MMT-x) with a force of 100 gf and dwell of 10 s with ASTM E-384 standard was used for the determination of the hardness of the sintered composite. Compression test was conducted at room temperature with the assistance of a universal testing machine (Instron 8801). The tests were carried out in accordance with the standards of ASTM E9. The length of each specimen was measured to be 16 mm, the diameter was measured to be 8 mm, and the length-to-diameter ratio was 2.0. The rule of mixture according to ASTM B962-15 was applied for the determination of the theoretical density of the composites. Determination of the density of the composites was made using the Archimedes principle and a Mettler Toledo equipment. The sessile drop analyzer is used for calculating the contact angles of composites while conducting wettability tests. The thermal diffusivity, specific heat and the thermal conductivity were measured by a hot disc using "Thermal constant analyser" (model number TPS 2500S)**.** Wear experiments were carried out using a pin-on-disc, at a speed of 0.1 m/s over a distance of 500 m, with applied loads of 5 N and 10 N. Prior to the wear test, a thorough cleaning was acetone was performed on the wear track specimens and composite specimens. The weight of each specimen was then calculated using a digital balance with accuracy of 0.001gm. The wear samples were cut to 8 mm diameter and 25 mm length by machining and finally polished. During the wear test procedure, the sample (pin) was maintained in a pressed position against a revolving EN31 steel disc, while a load that served as a counter weight was delivered, maintaining the balance of the pin. The weight of each specimen was calculated after the wear test. Thus, the amount of weight loss for each specimen was calculated. Electrochemical testing were carried out to investigate the composites' corrosion behaviour in 3.5% NaCI solution. A computer was connected to a Potentiostat testing device (model: Biologic SP-200) to conduct electrochemical testing. The EC-LAB software was utilised to analyse the electrochemical data. To determine the Potentiodynamic polarisation curve, the applied potential was varied from -10.0 V to + 10 V at a rate of 0.5 mV/min at room temperature.

3 Results and Discussion

3.1 Surface Morphology Analysis

3.1.1 Aluminium 7075 Alloy Reinforced SiC composites

Figure 4(a-e) SiC shows particles embedded in an aluminium matrix with uniform distribution. Figure 4(a) shows low reinforcement of 2 wt% SiC particles found in the space between the Al7075 matrix powders. Figure 4(a) and (b) relate to the agglomeration behaviour of the SiC particles. The FE-SEM image showed a uniform dispersion of the particles throughout the aluminium matrix. SiC particles were seen embedded in the surface of Al7075, while the matrix particle was deformed, causing a severe stress on the surface as shown in Fig. 4(f). With continuation of the mechanical alloying process, the new surfaces of SiC were exposed, due to fracture through repeated processing. Hence there was a decrease in particle size as shown in Fig. 4(g).

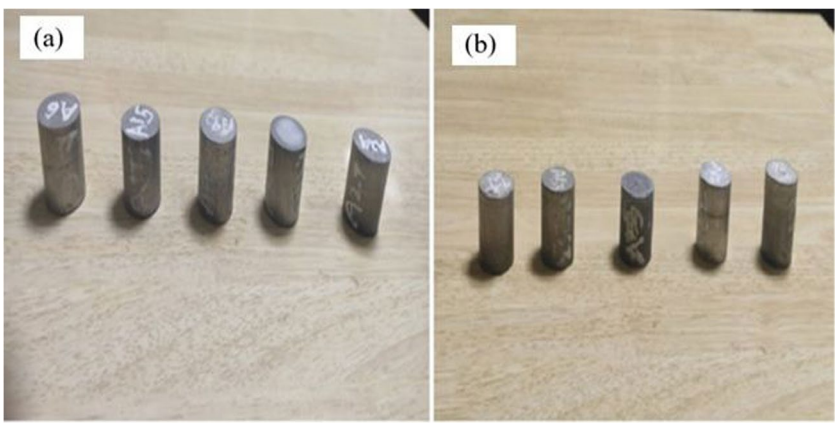

Fig. 2 Sintered composite samples **a** Al7075 + SiC **b** Al7075 + SiC + B_4C

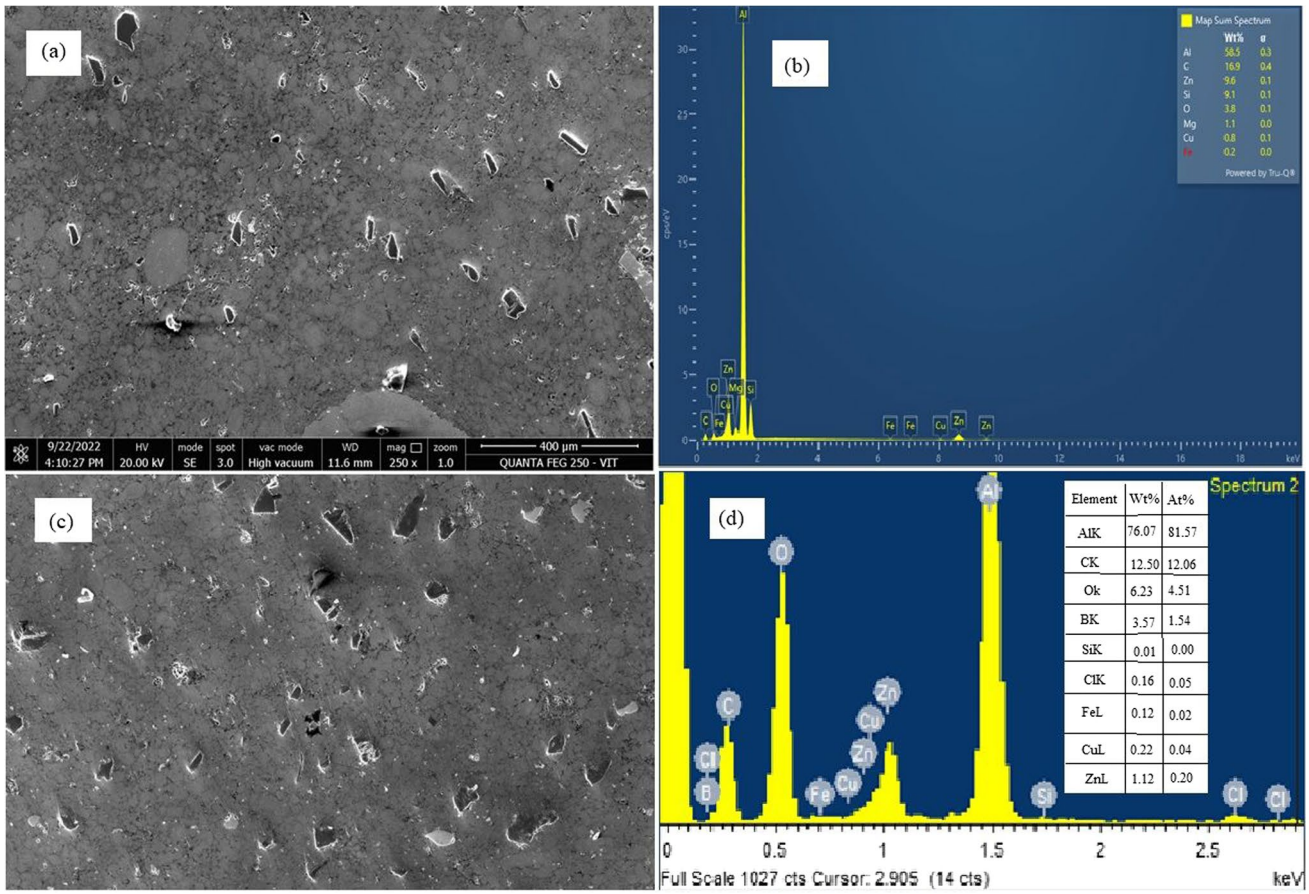

Fig. 3 **a** FESEM microstructure image of Al7075 + 4wt%SiC Composite **b** EDS analysis of Al7075 + 4wt%SiC Composite **c** FESEM microstructure images of Al7075 + 4wt%SiC + 2wt %B_4C composite **d** EDS analysis of Al7075 + 4wt%SiC + 2wt%B_4C composite

The particles tended to bond together, when the compacted specimens were sintered due to increase in grain boundaries. In general, changes occurring in particles' morphology was due to the mechanical alloying process. During the first stage of the process, the fracture and plastic deformation modes caused sliding of the powder particles over one another. In the second stage, the powder particles changed their shape due to a small amount of elastic and plastic deformation

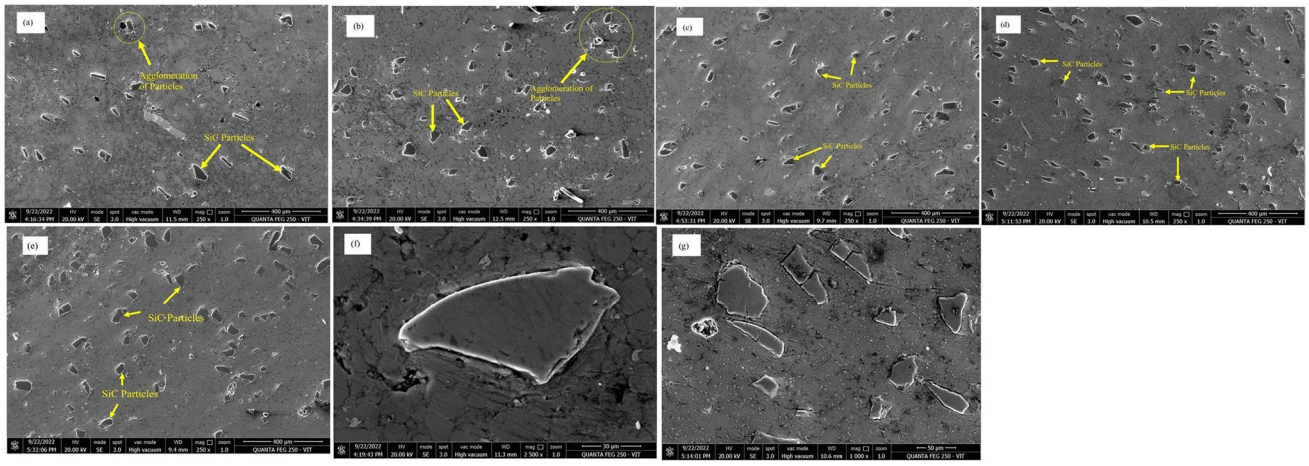

Fig. 4 FESEM image of Al7075 + SiC composite with different wt% of SiC **a** Al7075 + 2wt% SiC **b** Al7075 + 3wt% SiC **c** Al7075 + 4wt% SiC **d** Al7075 + 5wt% SiC **e** Al7075 + 6wt% SiC. **f** Morphology of SiC particle **g** Fracturing of SiC particles

and formed cold welding. The ductile–brittle nature of the Al–SiC powder produced by the mechanical alloying process was the primary cause of particle agglomerations. The findings demonstrated an increase in reinforcement wt% leading to the fragmentation of hard particles and homogeneous distribution due to the mechanical alloying effects [17, 18].

3.1.2 Aluminium 7075 Alloy Reinforced SiC and B_4C Composites

As shown in the Fig. 5(a-e), the dispersion of the reinforcement SiC and B_4C particles became homogeneous and had a smaller particle size due to the use of the mechanical alloying process. Figure 5(c) and (d) show the agglomeration behaviour of SiC and B_4C particles. The compacted specimens were seen having a tendency to gather into masses, when sintered, as a result of an increase in grain boundary and bonding. Increase in porosity occurred when the wt% of SiC particles increased from 4 to 6%. Variation in size was seen in the aluminium particles, which normally have a spherical form. On the other hand, the SiC particles often have angular morphologies and sharp corner edges. This could be due to high compaction loads sintered at 550 °C. The average particle size of the Al7075 + B_4C composite powders, which belong to the ductile–brittle system, was smaller than that of the Al7075 alloy powders, which belong to the ductile-ductile system; this difference might be attributed to an increase in the reinforcing component [19, 20].

3.2 EBSD Analysis

3.2.1 Aluminium 7075 Alloy Reinforced SiC Composites

Figure 6(a-c) shows the grain size orientation map, grain size distribution chart and inverse pole figure (IPF) chart from EBSD for Al7075 + 2wt%SiC composite. The grain size orientation map indicates that the composite grain boundaries are formed in a uniformly distributed pattern. Figure 6(b) shows the grain size distribution of Al7075 + 2wt%SiC composite with different grain sizes ranging from 1 µm to 10 µm and having 2.5 µm as average grain size. The inclusion of SiC particles results in a specific number of nucleation sites and enhanced the nucleation rate, which promoted grain refining and limited the development of Al grains, resulting in fine recrystallized grains. It is widely understood that the grain size that is achieved by the mechanical alloy process depends on the competition between the nucleation and growth rates [21]. These black points in the Fig. 6(a) may represent the unindexed points due to the porosity of the sample. The Fig. 6(d-f) represents orientation map, grain size distribution and IPF chart for Al7075 + 6wt% SiC composites. The addition of SiC particles leads to significant grain refinement, that was also observed in the grain size distribution graph. The Al7075 + 6wt%SiC composite microstructure had different grain sizes ranging from 1 µm to 10 µm, with an average grain size of 2.3 µm. It is evident from the colour orientation of grain size map that the Al7075 matrix grains are refined. Furthermore, the existence of strain plots

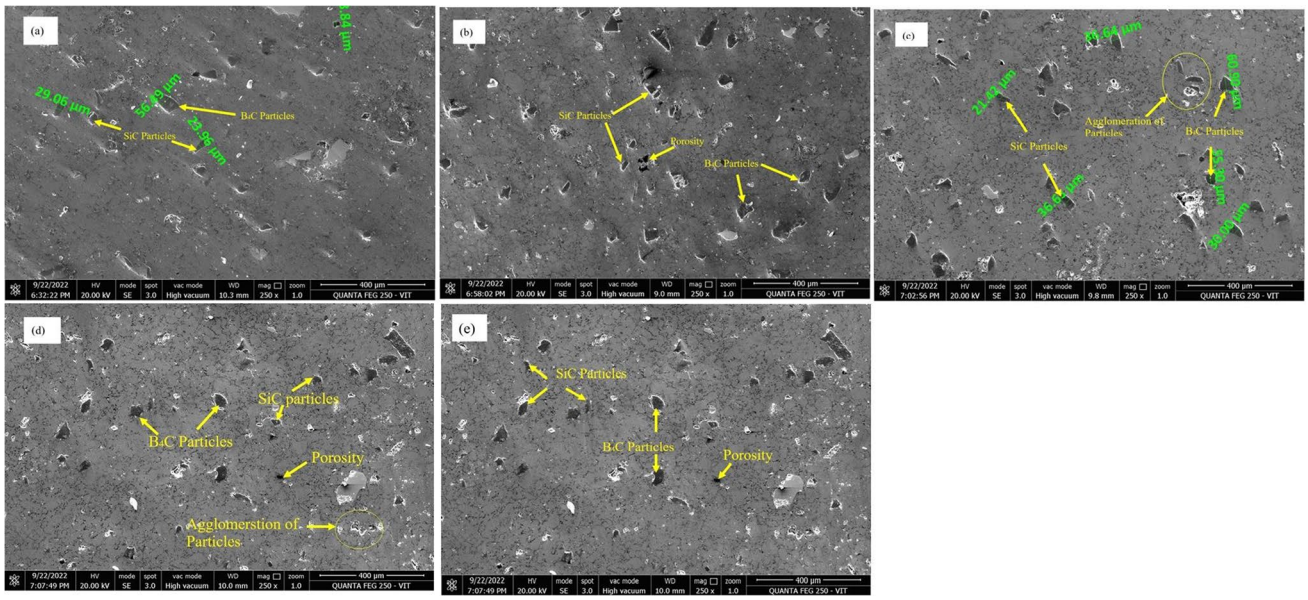

Fig. 5 FESEM image of Al7075 + SiC + B_4C composites with different wt% of SiC and constant 2wt% of B_4C. **a** Al7075 + 2wt% SiC + 2wt% B_4C **b** Al7075 + 3wt% SiC + 2wt% B_4C **c** Al7075 + 4wt% SiC + 2wt% B_4C **d** Al7075 + 5wt% SiC + 2% B_4C **e** Al7075 + 6wt% SiC + 2wt% B_4C

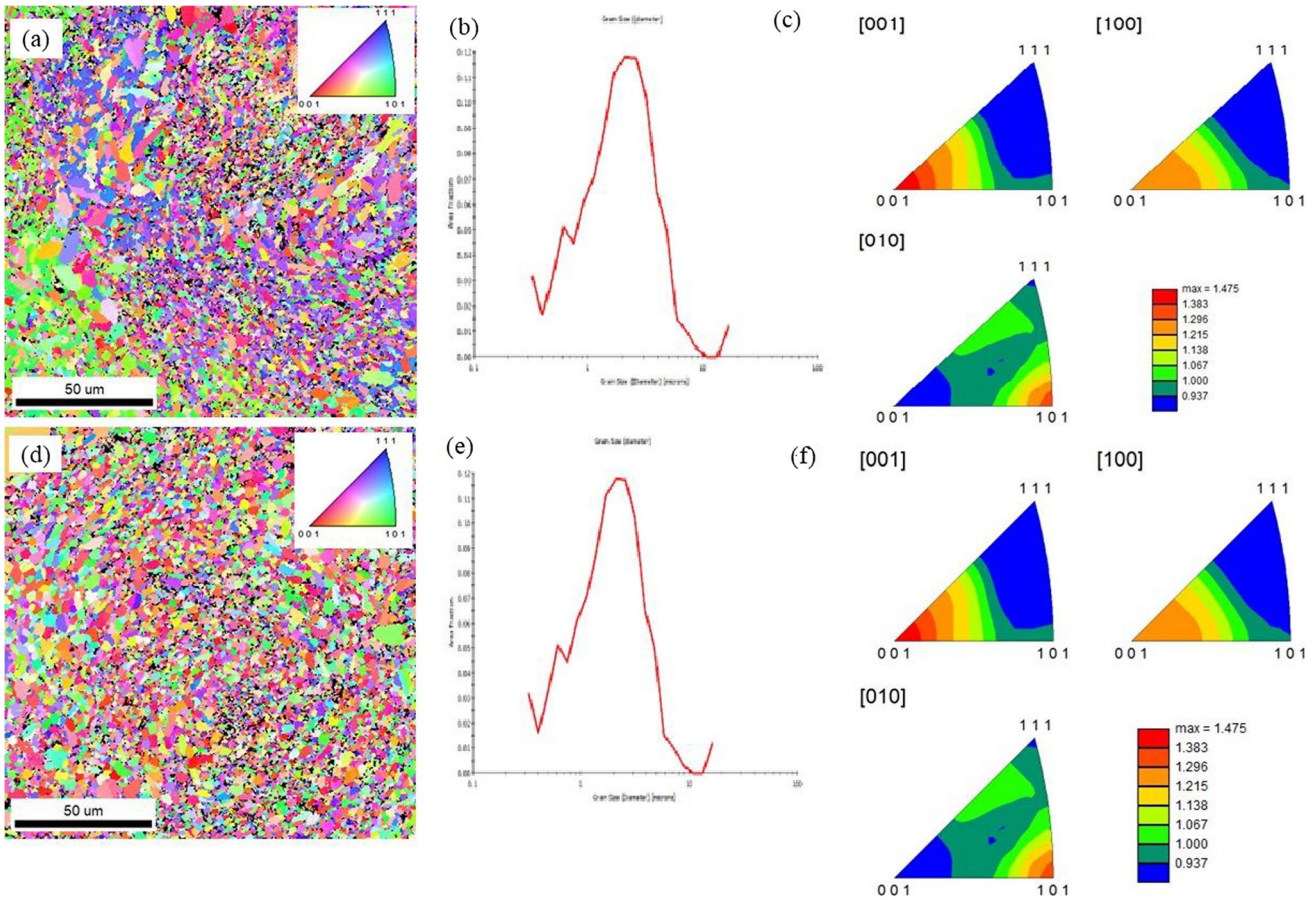

Fig. 6 Grain size orientation map, grain size distribution and IPF charts for the composites **a-c** Al7075 + 2wt% SiC **d-f** Al7075 + 6wt% SiC

with a greater quantity of dislocations is the key benefit to improve the mechanical characteristics that might be produced by the grain refining process. This is because strain fields tend to concentrate dislocations in areas of high stress [22]. Since the SiC particles were included with Al7075 alloy, the measured average grain size of the alloy began to decrease due to the pinning effect of the SiC particles.

3.2.2 Aluminium 7075 Alloy Reinforced SiC and B_4C Composites

The grain size orientation, grain size distribution chart, and IPF chart for Al7075 + 3wt%SiC + 2wt% B_4C and Al7075 + 4wt%SiC + 2wt% B_4C composites are displayed in Fig. 7(a-f). As shown in Fig. 7(b), the grain size distribution of the Al7075 + 3wt%SiC + 2wt% B_4C composite consisted of a variety of grain sizes ranging from 10 µm to 80 µm, with an average grain size of 19.06 µm. Figure 7(e) illustrates that the grain size distribution of the Al7075 + 4wt%SiC + 2wt%B_4C composite, which was composed of variety of grain sizes ranges between 20 µm and 100 µm, and having 21.65 µm as average grain size. The grain size orientation map that corresponds to hybrid composite sample composition displays a significant number of black dots, as shown in Fig. 7(a) and (d). The growing proportion of black spots or unindexed spots confirms that the porosity level increases steadily with increasing wt% of SiC with constant weight percentage of B_4C particles. Based on these findings, it is evident that the technique causes a considerable change in the powder's microstructure by decreasing the particle size. The increase in the grain boundaries density is a consequence of plastic deformation that occurs during the process. As a result of plastic deformation, there is a rise in the dislocation density at cell borders, which lead to a greater degree of misorientation between adjacent cells [23, 24]. The grain size colour orientation map, indicates that Al7075 + 3wt%SiC + 2wt%B_4C composites had better grain refinement than Al7075 + 4wt%SiC + 2wt%B_4C composites. As indicated by the EBSD analysis the grains in the Al7075 + 3wt%SiC + 2wt%B_4C composites are more refined than those in the Al7075 + 4wt%SiC + 2wt%B_4C composites, which leads to a higher microhardness value for the sample.

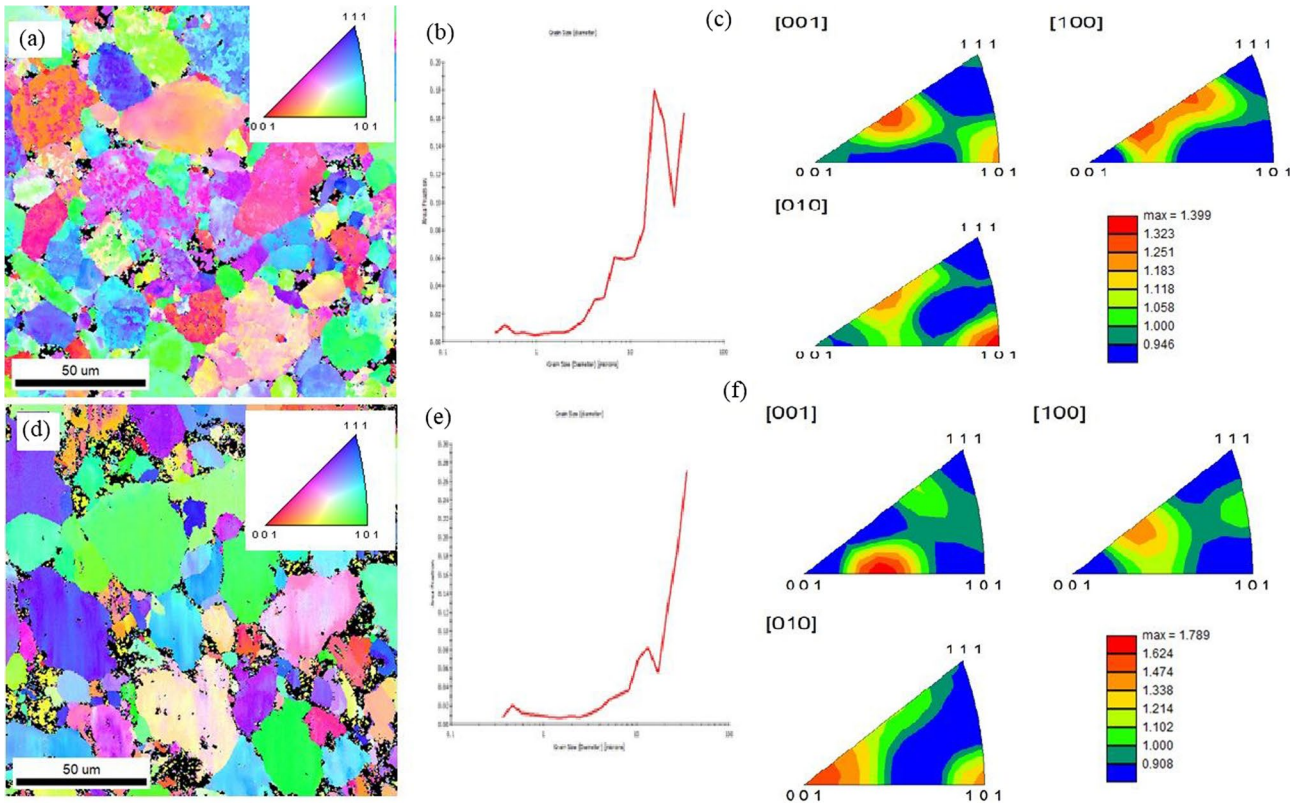

Fig. 7 Grain size orientation map, grain size distribution and IPF charts for the composites **a-c** Al7075 + 3wt% SiC + 2wt%B_4C **d-f** Al7075 + 4wt% SiC + 2wt%B_4C

3.3 X-Ray Diffraction Analysis

3.3.1 Aluminium 7075 Alloy Reinforced SiC Composites

Figure 8(a) illustrates the X-ray diffraction patterns of Al7075 + SiC composites produced using the PM technique. High peaks (111), (200), (311) and (222) were seen at 38.16°, 44.42°, 78.00° and 82.29° (2θ) for aluminium respectively. A very negligible peak observed at 2θ angle of 82.29° with miller indices of (112) confirmed the presence of Zn. The weak peaks (102), and (109) were obtained at 35.21° and 64.82° (2θ) for SiC respectively. The average crystallite size of aluminium ranged from 29.30 nm to 69.26 nm. while, the average crystallite size of SiC ranged from 38.20 nm to 56.46 nm. The average crystallite size of Zn peaks ranged from 29.00 nm to 56.46 nm. During the mechanical alloying process, a severe plastic deformation (SPD) of powder particles caused a decrease in the size of crystals based on aluminium to nanometres, as predicted. As a result, the dimensions of the matrix grains shrunk to less than 100 nm [25]. The mechanical alloying process resulted in the good formation of aluminium 7075 and SiC phases as established. The absence of oxide peaks in the XRD patterns was the evidence of the success of the powder metallurgy process in producing high-quality composite samples.

3.3.2 Aluminium 7075 Alloy Reinforced SiC and B_4C Composites

Figure 8(b) illustrates the X-ray diffraction patterns of Al7075 + SiC + B_4C composites were produced using the PM technique. High peaks (111), (200) and (222) were obtained at 39.19°, 45.42° and 83.20° (2θ) for aluminium respectively. Low intensity peaks (2θ) angle of 36.05° and 65.78° were obtained with miller indices planes of (102) and (109) respectively for SiC. A peak of negligible size was observed 43.82° (2θ) with miller indices of (109) for Zinc. A small peak observed at 2θ angle of 78.91° with miller indices of (119) confirmed the presence of B_4C. The average crystallite size of aluminium ranged from 14.70 nm to 29.17 nm, While the average crystallite size of SiC ranged from 27.00 nm to 27.47 nm. the average crystallite size of B_4C ranged from 41.00 nm to 41.82 nm. The average crystallite size of Zn ranged from 14.00 nm to 14.51 nm. The XRD patterns, helped identification of aluminium, zinc, SiC and B_4C peaks found. XRD analysis showed aluminium, the parent material as responsible for the most prominent peaks. The lower peaks of hybrid composites revealed their SiC and B_4C content. According to the XRD data, Al7075 did not undergo any new phase development, as indicated by this finding [26].

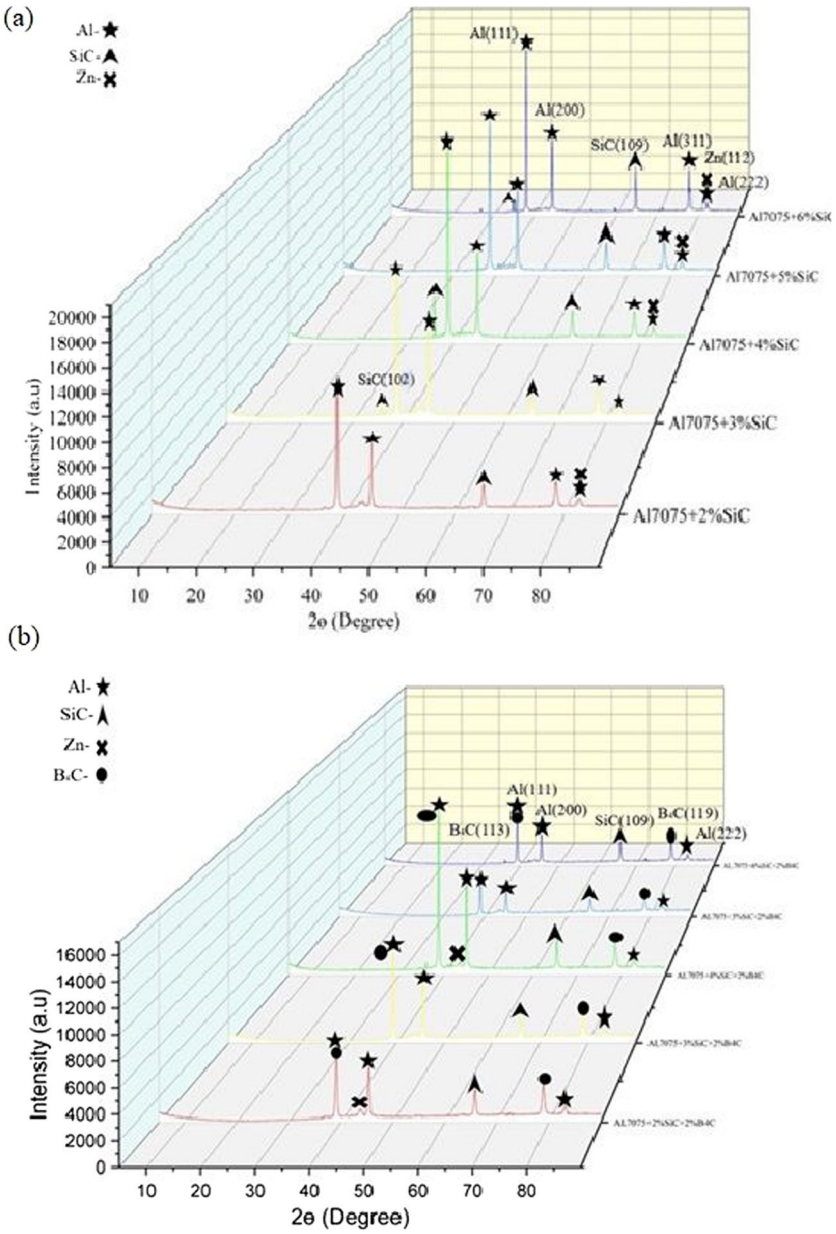

Fig. 8 **a** Phase analysis of Al7075 + SiC composites. **b** Phase analysis of Al7075 + SiC + B_4C composites

3.4 Hardness Analysis

3.4.1 Aluminium 7075 Alloy Reinforced SiC Composites

The hardness graphs of Al7075 + SiC composites shown in Fig. 9(a), indicate the composite material Al7075 + 6 wt% SiC with a substantially greater level of hardness compared to that of Al7075 + 2 wt% SiC. Increase in the wt% of SiC in the composite material was seen leading to an increase in the hardness of the material. Al7075 reinforced with 3 wt % and 4 wt % of SiC made a consistent improvement in hardness value from 126 to 143 HV respectively. Al7075 reinforced with 5 wt% and 6 wt% led to a rise in the hardness value from 162 to 195 HV respectively. Al7075 (6 wt % of SiC) sample achieved 41.5% higher hardness value (195 HV) than that of Al7075 reinforced with 2wt% SiC (114 HV). The inclusion of SiC transformed the ductile Al 7075 alloy into one with more brittle inherent characteristics. Acceleration of high degree of deformation can be done in mechanical alloying and grain size can be reduced to a finer level. Uniform distribution of SiC across the entire composite group may also play a role in its improvement of hardness. Sintering temperature is another factor that could contribute to the increased hardness of the composite material, due to an increase in temperature during the sintering process results in the strengthening of the bonds between the matrix and

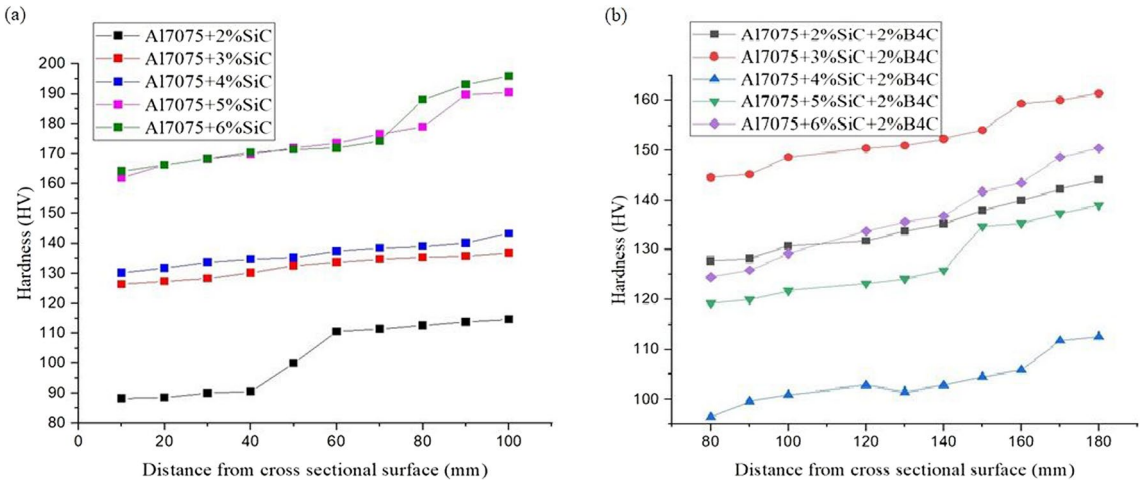

Fig. 9 **a** Cross sectional hardness value of Al7075 reinforced with different wt% of SiC composites **b** Cross sectional hardness value of Al7075 reinforced with different wt % of SiC and 2 wt % of B_4C composites

reinforcement particles. Incorporation of hard reinforcing particles, causes increase in strength and more resistance of the matrix leading to plastic deformation [27, 28].

3.4.2 Aluminium 7075 Alloy Reinforced SiC and B_4C Composites

Figure 9(b) shows the hardness graphs of Al7075 + SiC + B_4C composites. The presence of hard particles in a soft matrix like aluminium always enhanced hardness due to the existence of hard particles. Composite hardness value for Al7075 + 3wt%SiC + 2wt%B_4C achieved was 161 HV, 30.43% higher than that of Al7075 + 4wt%SiC + 2wt%B_4C (112 HV). The high hardness of ceramic particles caused enhancement of hardness due to the transfer of load to the ceramic particles through the matrix materials. However, when the particle size of the matrix material was too tiny, hard-reinforcement particles made a significant contribution to the increase. As a result, the link between the matrix and reinforcement, as well as porosity and voids, caused alterations in the final hardness value of the composites. The increased hardness of composites can be attributed to the following factors: (a) the existence of an intrinsic hard phase of boron carbide (B_4C) (b) the formation of irregularities in the composite structures as a result of reinforcements (c) enhancement of the dispersion effect as a result of homogeneous distribution of B_4C particles and (d) good bonding between the matrix alloy and the reinforcement. As a result of high porosity level, Al7075 + 4wt%SiC + 2wt%B_4C and Al7075 + 5wt%SiC + 2wt%B_4C composites had significant agglomeration results, which caused a significant reduction in the hardness value of the composites. The presence of B_4C particles increased the amount of local deformation, which ultimately resulted in improvement in particle welding. In addition, the increased local deformation imposed by the reinforcing particles increased the deformation hardening, which aids in the fracture process [29, 30].

3.5 Compression Analysis

3.5.1 Aluminium 7075 Alloy Reinforced SiC Composites

The sintered specimens were compressed for evaluation of strength. All the tests were performed at room temperature at a cross head speed of 2 mm/min. The samples were placed on the base plate, and then loaded until a fracture occurred. The reading of the load that was applied for the creation of a crack in the specimen was measured. This Fig. 10(a) illustrates the increase in compression strength that may be achieved by adding SiC particles to aluminium 7075 matrix. A greater compressive strength was achieved with increase in the SiC particles from 3 to 4% in the aluminium 7075 alloy. The impact of transmitting load from the ductile matrix to the reinforcement particles required a strong bond between the matrix and the SiC particles. A decrease in the space between the particles was seen during the fabrication of Al7075 + SiC composite particles by mechanical alloying. Consequently, there was an increase in the stress necessary to pass dislocations among reinforcement particles, resulting in a greater strength. By using powder metallurgy process, the aluminium particles were encased in SiC particles, which provided additional reinforcement. An excessive accumulation of these ceramic particles, during the compaction process, caused restriction in the mobility of these brittle, hard and elastically deforming ceramic particles. Composites with high pore levels have a lower compression strength. There may be a reason for the decrease in compression strength in Al7075 alloy composites with a larger

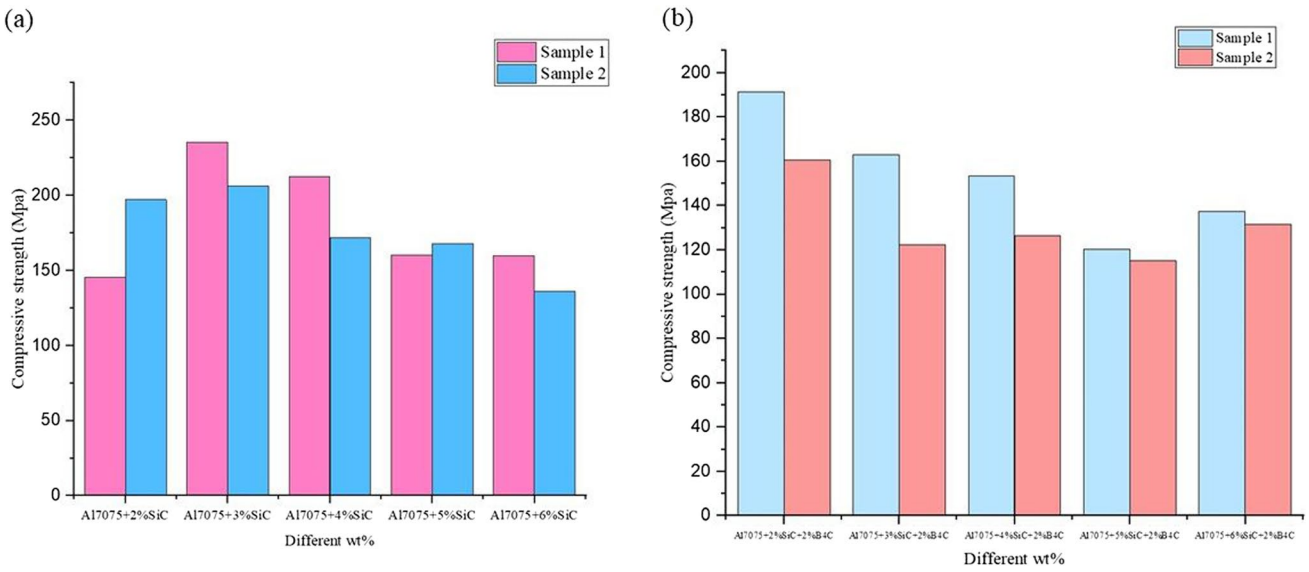

Fig. 10 **a** Compression analysis of Al7075 + SiC Composites **b** Compression analysis of Al7075 + SiC + B_4C Composites

wt% of reinforcement (5 and 6 wt%). The presence of pores caused stress concentration sites, which ultimately resulted in the formation of cracks at the interface regions between the pore-reinforcement matrix. Coalescence of these cracks causes he composite material to fracture prematurely [31].

3.5.2 Aluminium 7075 Alloy Reinforced SiC and B_4C Composites

The inclusion of silicon carbide and boron carbide particles led to an increase in the compression strength of the Al7075 material, as shown in Fig. 10(b). The matrix alloy demonstrated better compressive strength when the weight percentage of SiC was increased from 2 to 4%, The wt% of B_4C reinforcement particles was held constant at 2 wt%, which are quite hard on their own, could be the cause for the increased hardness seen in the composite. The increased hardness of the Al7075 + SiC + B_4C composites was also due to the uniform distribution of SiC that occurs during the formation of the composites. Dispersion strengthening mechanism is the most important strengthening mechanisms to raise the strength of the composite. During the process of densification, the high concentration of B_4C particles resulted in agglomeration of particles, which impedes the development of a dense sample. Agglomerated B_4C particles not only impeded the process of appropriate densification, but also served as fracture initiation sources, which ultimately leads to the quick failure of composites [32, 33]. This could be the cause of the reduction in compression strength that was observed in Al7075 alloy composites that had a higher wt% of reinforcement (Al7075 + 5wt%SiC + 2wt%B_4C).

3.6 Density Analysis

3.6.1 Aluminium 7075 Alloy Reinforced SiC Composites

The difference between the experimental density and the theoretical density of Al7075 + SiC composites is shown in Fig. 11(a). Theoretical, calculations were made of the densities of AMC were carried out by utilising the mixing rules.

$$\text{Theoretical density} = (\rho \text{ of Al alloy} \times \text{wt\% of Al alloy}) + (\rho \text{ reinforcement} \times \text{wt\% of reinforcement}) \quad (1)$$

The experimental density was determined using the Archimedes principle in accordance with the ASTM standard B962-15.

$$\rho_c = \frac{W}{W - W1} \times \rho_w \quad (2)$$

ρ_w density of pure water
ρ_c density of Fabricated part
W Weight of composite in air
W_1 Weight of composite in water

$$\text{Relative density} = \text{Experimental density}/\text{Theoretical density} \times 100 \quad (3)$$

The highest relative density value of 93% was obtained for Al7075 + 2wt%SiC composite and the lowest relative density value of 86% was achieved for Al7075 + 6wt%SiC composite, as shown in Fig. 11(b). The theoretical density values of the composites were somewhat higher than those of the experimental density values of the composites.

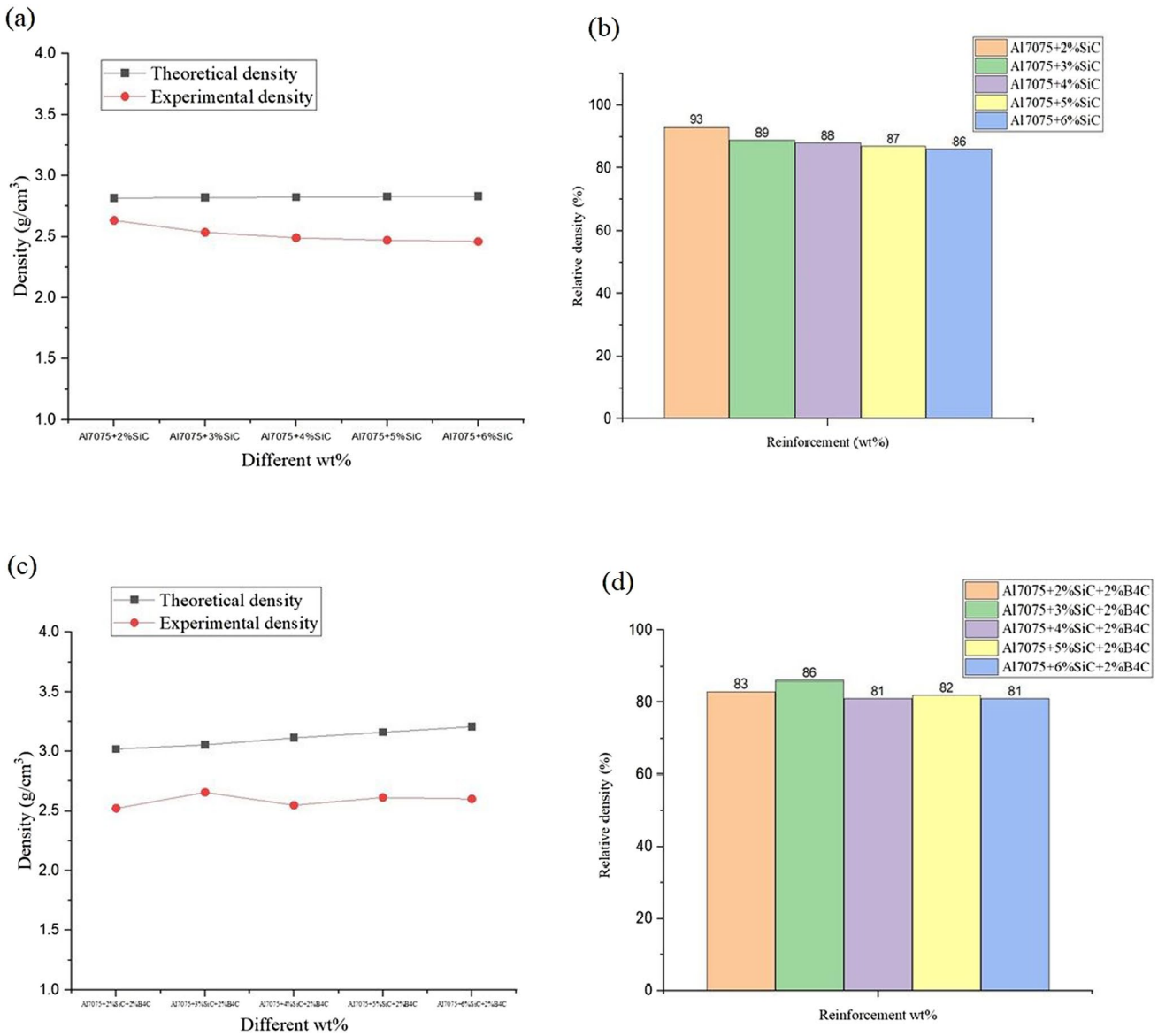

Fig. 11 **a** Density analysis of Al7075 + SiC composites **b** Relative Density analysis of Al7075 + SiC composites **c** Density analysis of Al7075 + SiC + B_4C composites **d** Relative Density analysis of Al7075 + SiC + B_4C composites

Increase in the wt% of SiC in composites resulted in a higher density of the composites. This was due to the powder particles being in their sliding stage throughout the pressing process, and the continued movement of the powder particles during the pressing process, with the continuous filling of the pores. As a result, an increase in pressure caused achievement of the highest possible value in the Al7075 + SiC relative density of the particles [34].

3.6.1.1 Aluminium 7075 Reinforced SiC and B_4C Composites Figure 11(c) shows a comparison between the experimental density and the theoretical density of Al7075 + SiC + B_4C composites. As seen in Fig. 11(d), the composite made of Al7075 + 3wt%SiC + 2wt% B_4C had the highest relative density value of 86%, while the composite made of Al7075 + 6wt% SiC + 2wt%B_4C had the lowest relative density value of 81%. The irregular forms of the matrix material, which were filled by reinforcement powders, increased the porosity values of the composites. The presence of brittle particles (B_4C) reduced the density of the materials. It is widely known that the mechanism of powders compacted in a rigid die is typically broken down into three steps, which include the following: (i) sliding and rearranging of the particles' positions (ii) elastic deformation of ductile particles and the fracture of brittle solids and (iii) deformation of bulk compressed particles into plastic form [35 36].

3.7 Porosity

3.7.1 Aluminium 7075 Alloy Reinforced SiC Composites

The porosity of Sintered composites was calculated by using

$$\text{porosity}(\%) = \frac{\text{Theoretical density} - \text{Experimental density}}{\text{Theoretical density}} \times 100 \quad (4)$$

Optical Microscope images indicated the presence of high pores in the Al7075 + 6wt%SiC, with the presence of low pores in the Al7075 + 2wt%SiC composite, as shown in Fig. 12(a) and (b). There was an increase in the porosity values of composites as a result of an increase in the wt% of SiC in the composites as shown in Fig. 13(a). The inability of the matrix and the particles to interact with one another through the medium of wetting was the primary cause for the increased porosity found in the composites. Increase in the porosity values of the composites found could be be attributed to the irregular shape of matrix material filled with reinforcement powders [37, 38].

3.7.2 Aluminium 7075 Alloy Reinforced SiC and B_4C Composites

Optical Microscope images indicated presence of the high pores in the Al7075 + 6wt%SiC + 2wt%B_4C, while low pores were present in the Al7075 + 3wt%SiC + 2wt%B_4C composite, as shown in Fig. 12(c) and (d). The inclusion of reinforcements resulted in the average rise in the porosity values of the reinforced hybrid composites as shown in Fig. 13(b). The increasing porosity level in aluminium composites was due to the intrinsic characteristics of B_4C particles, which were harder compared to the matrix phase and developed some amount of clustering of particles in high content of reinforcement into a composite that is incompressible and would resist during compaction. There was also a correlation between the concentration of the B_4C particle and an increase in the contact area of the particle. Further, during the sintering process, both surfaces were seen affected by the mismatch in thermal coefficients between the matrix alloy and the B_4C reinforcement [39, 40]

3.8 Wettability Analysis

3.8.1 Aluminium 7075 Alloy Reinforced SiC Composites

A sessile drop image on the surface of aluminium 7075 alloy-reinforced SiC composites as shown in Fig. 14(a-e). Aluminium 7075 composites (Al7075 + 2wt% SiC) were tested with water, and the findings indicate that the average contact angle with S.D was 63.87° ± 0.19°. The

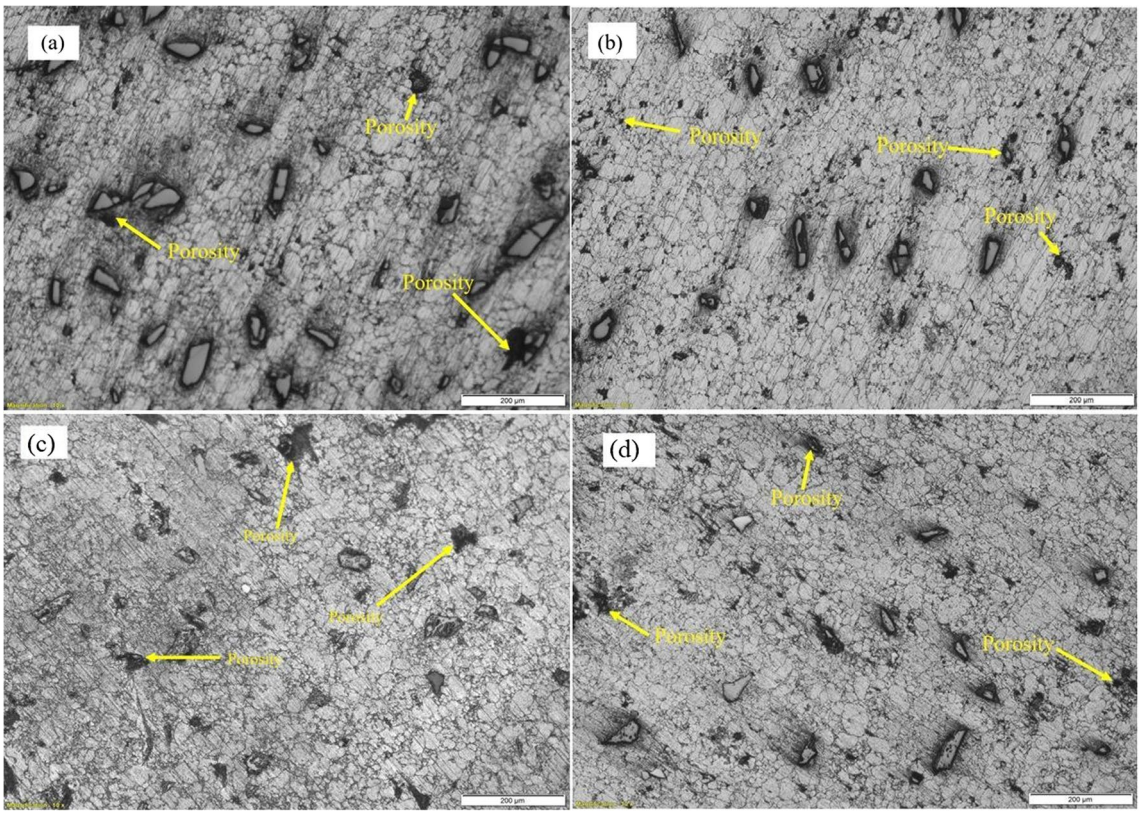

Fig. 12 Optical microscope images **a** Al7075 + 6wt%SiC composite **b** Al7075 + 2wt % SiC composite **c** Al7075 + 6wt%SiC + 2wt%B_4C composite **d** Al7075 + 3wt%SiC + 2wt%B_4C composite

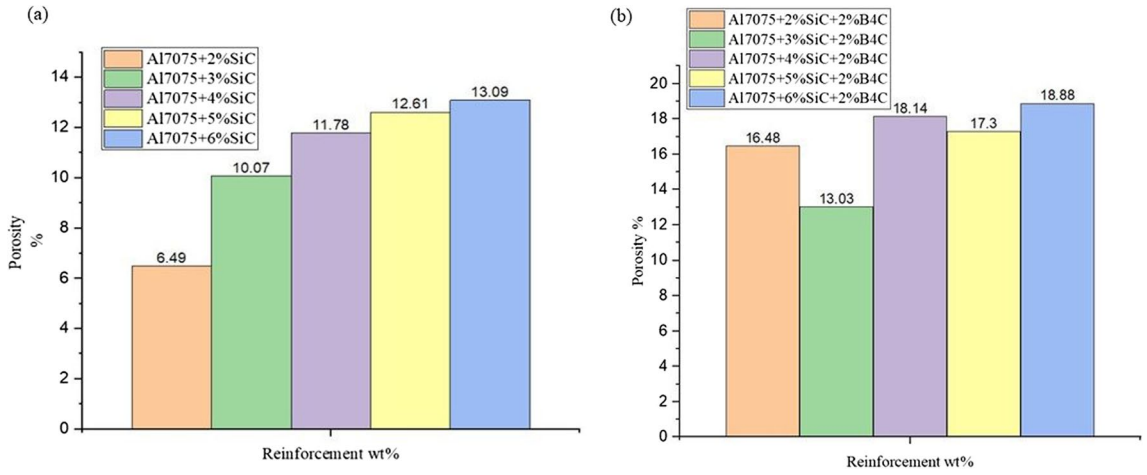

Fig. 13 Porosity values **a** Al7075 + SiC composites **b** Al7075 + SiC + B_4C composites

different contact angle was measured for the Al7075 reinforced with different wt% of SiC (2wt% to 6wt%). The value of the contact angle 63.87° indicates that the surface of the (Al7075 + 2wt% SiC) composite behaves like a hydrophilic. Because the Si surface tension is lower when compare to Al, the Si can refine at the drop surface, resulting in reduced surface tension of the composite. According to the contact angles, the reduction in surface tension has relatively less influence on the wettability of the substance. As shown in Fig. 14(e) the hydrophobic nature of the composite was achieved by adding the amount of SiC to aluminium 7075 alloy. With the addition of 6wt%SiC (Al7075 + 6wt%SiC), the contact angle was improves to 93.96° ± 0.70°, as shown in Fig. 14(e). The silicon layer produced on the contact surface of SiC particles on aluminium 7075 composites is expected to have 2 roles. First, it is expected to shield the SiC from the attacks of aluminium and the production of Al_4C_3, and second, it is to increase the wettability of aluminium, which should resist the interaction between aluminium and the SiO_2 layers [41, 42]. However, the nominal Al7075 + 6% SiC composite spread faster than Al7075 + 2wt%SiC composite. Most likely this

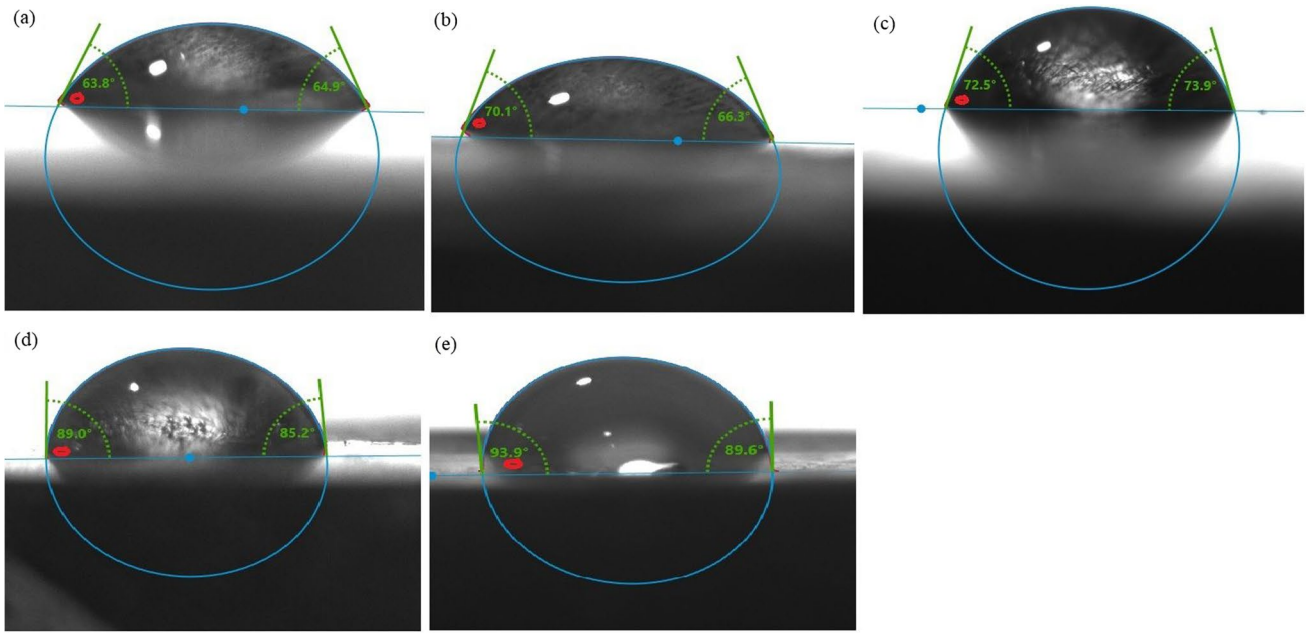

Fig. 14 Optical images of sessile drop on Al7075 composites **a** Al7075 + 2wt%SiC **b** Al7075 + 3wt%SiC **c** Al7075 + 4wt%SiC **d** Al7075 + 5wt%SiC **e** Al7075 + 6wt%SiC

was because the nominal Al7075 + 6wt% SiC composite had a lower viscosity at the eutectic composition.

3.8.2 Aluminium 7075 Alloy Reinforced SiC and B_4C Composites

The Fig. 15(a-e) illustrates the sessile drop image of the hybrid aluminium 7075 composites. The average values of the hybrid composite's (Al7075 + 2wt%SiC + 2wt%B_4C) water-based contact angle improved substantially to 76.94°. Due to the addition of SiC and B_4C, the surface of the composites become hydrophilic, with a standard deviation of 1.59°. The various contact angle are measured using sessile drop experiment for hybrid Al7075 reinforced with different wt% of SiC (2wt% to 6wt%) and constant B_4C(2wt%) as shown in Fig. 15(a). The average contact angle of Al7075 + 3wt%SiC + 2wt% B_4C has increases to 102.34°, resulting in the composite's hydrophobic in nature as shown in Fig. 15(b). This is because, as the wt% of SiC increases, the polarity of the surface material reduces, indicating that a decrease in surface energy and an increase in hydrophobicity. The alloying of aluminium with magnesium helps to break the oxide films at the surfaces of both the aluminium droplets and the SiC particles, which in turn promotes an improvement in wettability [43, 44]. It is feasible to determine that the presence of SiC and B_4C in the fabrication of aluminium 7075 composites not only contributes the strengthening the matrix material but also protect oxygen from the contact surface of the particle, which increases the surface intensity of the particles.

3.9 Thermal Conductivity Analysis

3.9.1 Aluminium 7075 Alloy Reinforced SiC Composites

As shown in Fig. 16, experiments were carried out by utilising the thermal constant analyser order to determine the thermal conductivity (K) and thermal diffusivity of Al7075 matrix composites. The cylindrical specimens with dimensions of 26 mm diameter and 25 mm height were used for the testing. The composite with low wt% and high wt% of reinforcement were subjected for thermal constant analyser to determine the thermal conductivity, thermal diffusivity and specific heat values and are present in Table 4. The Al7075 + 6wt%SiC Composite has attained the maximum thermal conductivity value as 58.99 W/mK. This happens due to the fact that the mobility and acceleration of electrons inside the morphology are the primary causes that determine the thermal conductivity of the metal matrix composites. Because SiC particles have a greater electron acceleration, heat can diffuse more quickly in them [45, 46]. The lower 'K' was obtained for Al7075 + 2wt%SiC Composites as 56.47

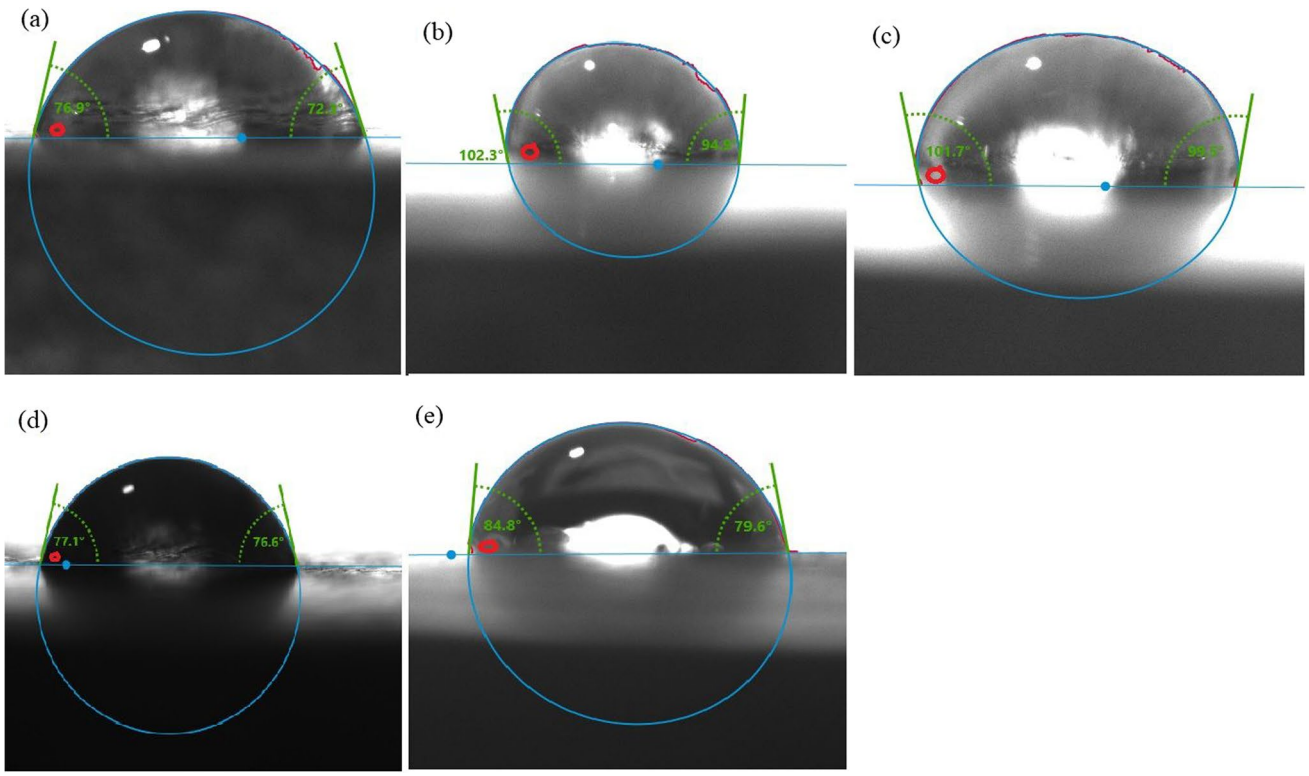

Fig. 15 Optical images of sessile drop on Al7075 hybrid composites **a** Al7075 + 2wt%SiC + 2wt%B_4C **b** Al7075 + 3wt%SiC + 2wt%B_4C **c** Al7075 + 4wt%SiC + 2wt%B_4C **d** Al7075 + 5wt%SiC + 2wt%B_4C **e** Al7075 + 6wt%SiC + 2wt%B_4C

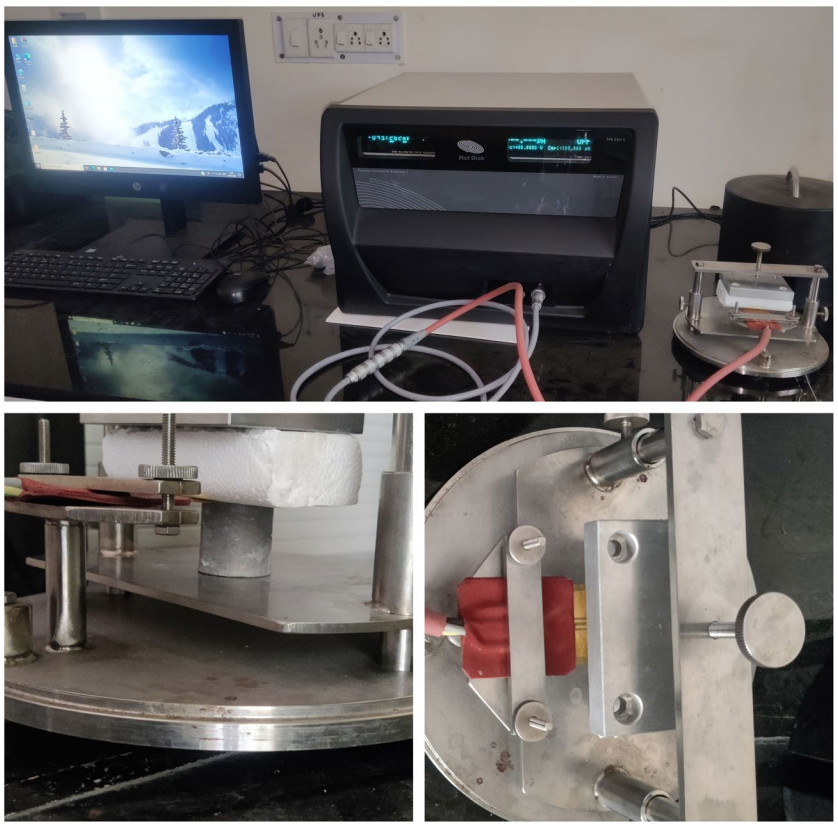

Fig. 16 Computerized thermal constant analyser equipment

W/mK. The significant factor that contributes to the decrease in 'K' of the composites was due to smaller grain size of SiC and lesser grain size of matrix material. This leads to an increase in the grain boundaries resistance.

3.9.2 Aluminium 7075 Alloy Reinforced SiC and B_4C Composites

The values of thermal conductivity, thermal diffusivity, and specific heat that were measured are listed in Table 5. The Al7075 + 2wt%SiC + 2wt%B_4C composites has reached the highest thermal conductivity (K) value of 58.67 W/mK, while the Al7075 + 6wt%SiC + 2wt%B_4C composites has reached the lowest thermal conductivity (K) value of 52.99 W/mK. Interface cracks and a reduction in the original contact among the two surfaces are known as geometric deviations in the crystal structure (lattice mismatch). In fact, heat transfer at an actual intersection between two surfaces act in a identical aspects to 'K' in solids, but heat transmission in a gap act in a identical aspect to 'K' in a fluid. This gap blocks the passage of electrons and phonons across the contact, preventing their movement in both directions. When reinforced particles are smaller in size, there are more thermal limits in the interface area between matrix and particles [47, 48]. This results in a lower thermal conductivity in the composite. Another important factor is porosity, diminish the 'K' of the composite, due to the effect of pace at which heat is transferred through the composite, and in fact it works as an interface by producing thermal resistance.

3.10 Tribological Analysis

3.10.1 Aluminium 7075 Alloy Reinforced SiC Composites

In this study, the wear rates of Al7075 reinforced SiC composites were examined in relation to the sliding distance by altering the applied loads as 5N and 10N. Two samples were tested

Table 4 Measurement of thermal conductivity, thermal diffusivity and specific heat of Al7075 reinforced SiC composites

S No	Sample Details	Thermal Conductivity (W/mK)	Thermal Diffusivity (mm^2/s)	Specific Heat (MJ/m^3k)
1.	Al7075 + 2wt%%SiC	56.47	15.88	3.557
2.	Al7075 + 6wt%%SiC	58.99	27.03	2.183

Table 5 Measurement of thermal conductivity, thermal diffusivity and specific heat of Al7075 reinforced SiC and B_4C composites

S No	Sample Details	Thermal Conductivity (W/mK)	Thermal Diffusivity (mm^2/s)	Specific Heat (MJ/m^3k)
1.	Al7075 + 2wt%SiC + 2wt%B_4C	58.67	12.80	4.582
2.	Al7075 + 6wt%SiC + 2wt%B_4C	52.99	14.35	3.693

for each trial and the average value was calculated and depicted as shown in Fig. 17(a). The wear rate of the specimen was analysed using the approach that involved the loss of weight and the sliding distance can be calculated by dividing the weight lost over the duration of a specified distance. With increase in the applied load, the contact pressure and temperature between the pin and the disc also increased. This caused plastic deformation in the pin surface, which allowed the sliding surface of the pin to adhere to the disc, resulting in a greater amount of material being removed. When the load was increased from 5 to 10 N, there was a corresponding rise in the wear rate of the composites. Variation in wear increased over time under higher load over the specimens. The inclusion of the SiC particles results in a significant reduction in the wear rate of the composites. The composites made of Al7075 + 2wt% SiC were seen having a lowest wear rate, While the Al7075 + 3wt% SiC was seen having a high wear rate, when loaded with 5N over a 500 m sliding distance as shown in Fig. 17(a). The composites made of Al7075 + 4wt% SiC were found having the lowest wear rate and the Al7075 + 3wt% SiC was found to have a high wear rate, when loaded with 10N as shown in Fig. 17(a). SiC particles also exhibited excellent bonding and did not become detached from the matrix during testing. It is possible for SiC to get entrapped between the sliding surfaces or entrenched in the soft aluminium matrix, which results in increased wear resistance. In the initial stages of the wear process, the contact between the asperities on the EN31 disk and the composite pin could have resulted in in the fragmentation and fracture of SiC, leading to the transfer of materials inside the tribosystem. On the other hand, the sharp edges of the ceramic reinforcement particles that stand out of the composite surface had the potential to cut the steel disc surface and produce a small iron fragments. This can occur, due to irregular surface of the composite pin. As a result, wear debris can become trapped between the two sliding surfaces and be subjected to intense compressive forces created by the moving surfaces. The wear debris were shattered as a result of compressive stress mixed, and compressed, which ultimately resulted in the formation of mechanically mixed layer (MML). The wear resistance of the composite with lower loads is superior to that of composite with higher loads [49, 50].

3.10.2 Influence of Al7075 + SiC wt% on Coefficient of Friction

The friction coefficient of Al7075 composites with varied applied loads of 5N and 10N with a fixed sliding distance of 500 m is displayed in Fig. 18(a) and (b). At the beginning of

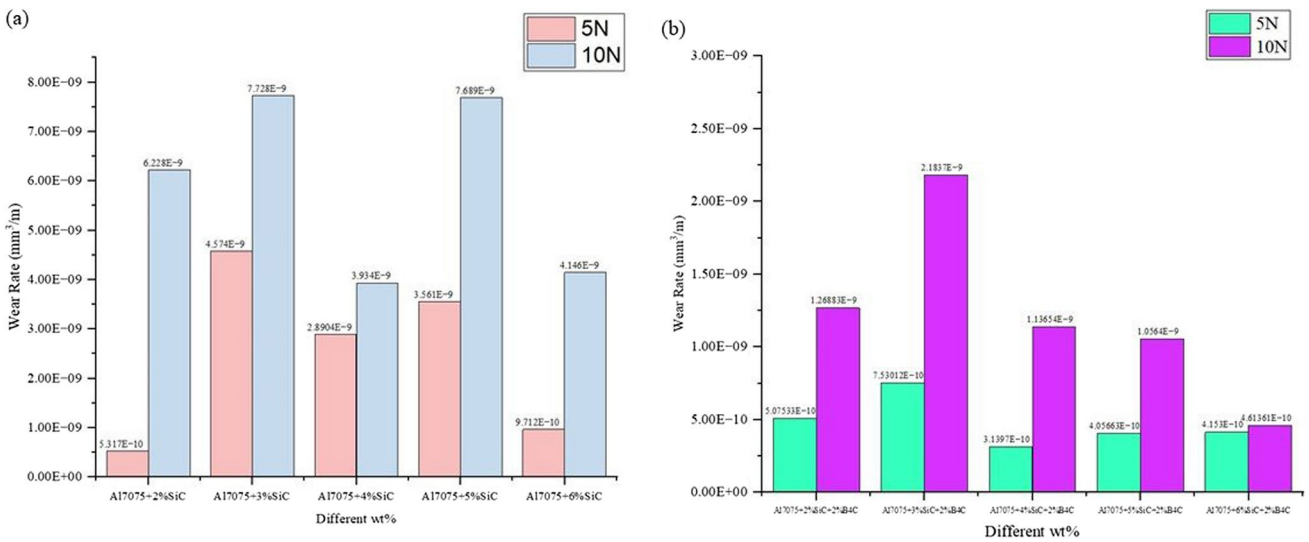

Fig. 17 **a** Wear rate of Al7075 + SiC composites with respect to sliding distances of 500 m under loads of 5N and 10 N. **b** Wear rate of Al7075 + SiC + B_4C composite with respect to sliding distances of 500 m under loads of 5N and 10 N

the experiment, the friction coefficient of all the specimens reached their peak values, followed by a fell till reaching a relatively stable value. As a result, greater friction coefficient was caused by an increase in the amount of friction force required break the extremely adhesive contact that existed between the tested surfaces. The subsequent reduction in the friction coefficient could have been caused by the creation of the mechanically mixed layer on the surface.

3.10.3 Wear Mechanism Analysis of Worn Surface

The Al7075 + 4wt%SiC samples of 10N were found to be effective in achieving the desired low wear rate. Hence, the worn surfaces of the Al7075 + 4wt%SiC specimens were examined using SEM in order to define the wear processes, revealing that the wear mechanisms varies based on the wear conditions (Namely, the load and the sliding distance). After a sliding distance of 500 m, abrasion wear reveals on the previously worn surface as shown in Fig. 19(a). It is necessary to have a sliding length of at least 500 m to develop, deformation and delamination wear process. The delamination wear mechanisms can be viewed as removal of material due to the appearance of fracture in areas where the delamination occured. Al7075 + 3wt%SiC Composites exhibit larger deformation zones at a sliding distance of 500 m, as illustrated in Fig. 19(b). Application of increased force caused increased in hardening leading to the formation of fractures in the contact area between the matrix and the reinforcements [51, 52].

3.10.4 Aluminium 7075 Alloy Reinforced SiC and B_4C Composites

The wear test was performed on two samples for each trial, and the average value was calculated and depicted in Fig. 17(b). The wear rate increased in proportion to the applied force as well as the wear distance in each sample. The composites made of Al7075 + 4wt% SiC + 2wt%B_4C was found to have a lowest wear rate and the Al7075 + 3wt% SiC + 2wt%B_4C was found to have a high wear rate, when loaded with 5N over a 500 m sliding distance as shown in Fig. 17(b). The composites made of Al7075 + 6wt%SiC + 2wt%B_4C was found to have the lowest wear rate and the Al7075 + 3wt% SiC + 2wt%B_4C was found to have a high wear rate, when loaded with 10N as shown in Fig. 17(b). The findings showed, Aluminium 7075 hybrid composites with display of greater abrasion resistance at all temperature, as well as greater thermal stability, which could be attributed to the evenly dispersion in SiC and B_4C particles. The wear rate of the composites was significantly improved by the inclusion of the reinforcing particles, and lowered through increase in the weight fraction of SiC and B_4C in the composite. The enhancement of the wear resistance of the Al7075 + SiC + B_4C composite depended heavily on its increased hardness. The presence of B_4C particles made a substantial enhancement in the hardness of the composite, which resulted in a low wear rate of the composite, as shown in Fig. 17(b). During the dry sliding process, B_4C fulfilled the function of the load-bearing function. The absence of reinforcement in the Al7075 matrix, experienced the greatest amount of wear-related mass loss. During the wear process, the large quantity of B_4C content resulted in high hardness, which led to the composite having the lowest wear rate. The Al7075 composite pin and disc material (counter material) slide against each other under increased load, causing both surfaces to reach higher temperatures. As a consequence, the protective layer (MML) will be reduced, and B_4C reinforcement will strengthen the soft alloy. As a result, there was an increase in the wear rate of the composite. However, compared to the higher load composite, the low loads composite reinforced with SiC and B_4C particles demonstrated superior wear resistance. The improvement in wear rate can be attributed to an increase in hardness, specifically the increased hardness of SiC and B_4C, as well as the pinning of dislocations by these hard particles. The resistance provided by the dispersed particle during sliding resulted in a lower wear rate of the composites. Due to the high degree of subsurface cracking that occurred under the transition load, the mechanically mixed layer eventually wear out and disappeared under these conditions. During the time when the B_4C particle emerged from the sliding surface, a majority of the load carried by the composite surface was carried by the B_4C particle. It is commonly known that the lower frictional coefficient (steel and B_4C) than steel and aluminium alloy. Hence, the inclusion of B_4C reinforcement to Al7075 + SiC composites increased the material's wear performance [53, 54].

3.10.5 Influence of Al7075 + SiC + B_4C wt% on Coefficient of Friction

The friction coefficients of Al7075 hybrid composites under varying applied loads of 5N and 10N with a fixed sliding distance of 500 m are shown in Figs. 18(c) and (d). The following factors were responsible for the changes in the friction coefficient: At the beginning of the process, when two surfaces touched and began slide, a force of friction was produced. Figure 18(c) and (d), show a decrease in the coefficient of friction with an increase in the amount of SiC and B_4C particles under the load of 5N, preventing a blunting or breaking of the surfaces under load. B_4C impacts the coefficient of friction due to the formation of boron oxide (B_2O_3) layer at the contact zone. The B_4C particles are easily drawn out and react with the atmosphere, causing the formation of the (B_2O_3) oxide layer [55].

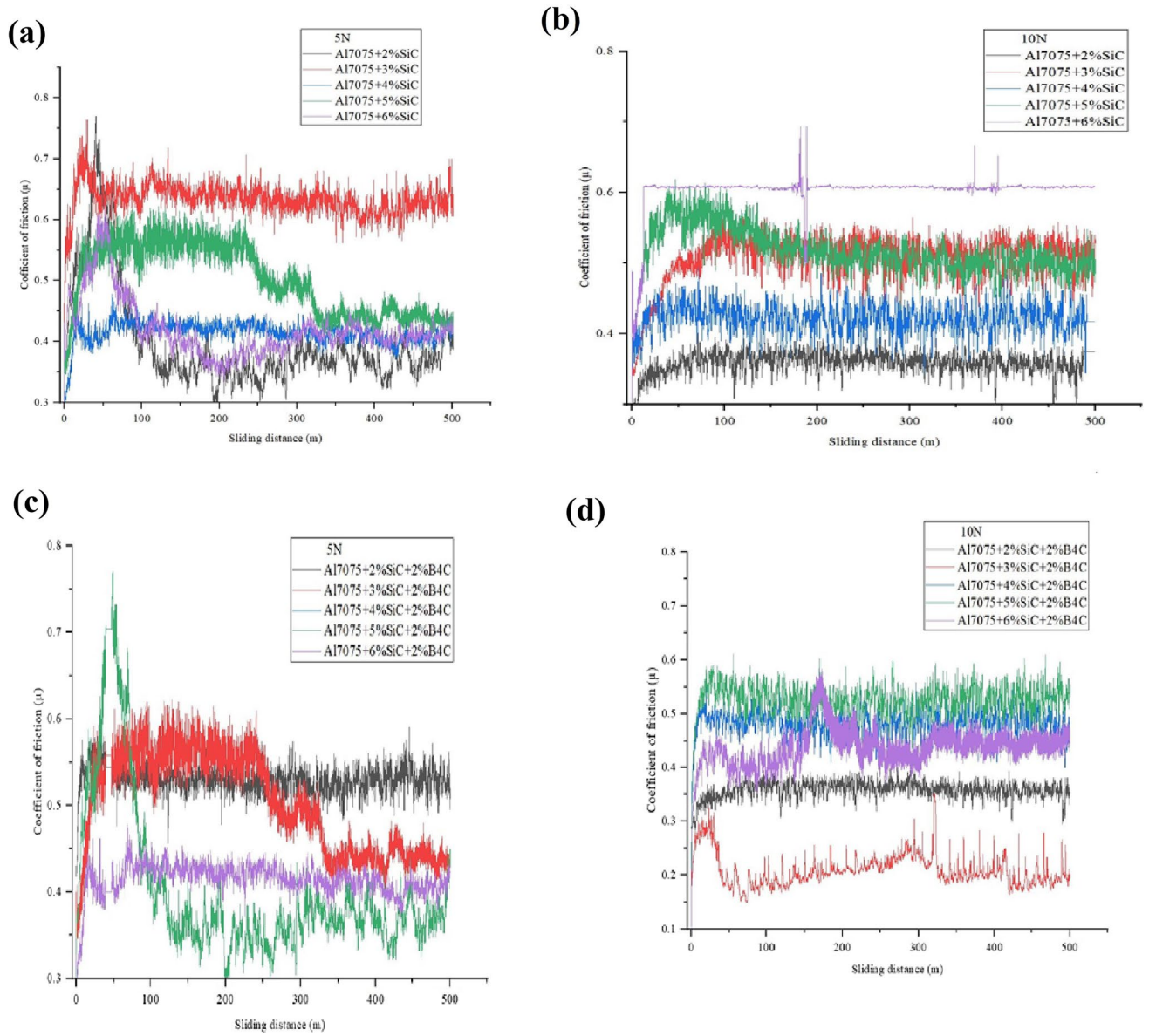

Fig. 18 Coefficient of friction of Al7075 + SiC composites with respect to their sliding distance. (**a**) 5N (**b**) 10N. Coefficient of friction of Al7075 + SiC + B_4C composites with respect to their sliding distance (**c**) 5N (**d**) 10N

3.10.6 Wear Mechanism Analysis of Worn Surface

A considerable amount of granular wear debris and grooves indicated micro-cutting and abrasive wear as the predominant wear processes, as shown in Fig. 19(c). The addition to grooves and granular wear debris multiple delamination layers helped getting stuck to the worn surfaces as the sliding distance increases as shown in Fig. 19(d). The abrasion was seen as severe in Al7075 + SiC + B_4C composites, due to the presence of dislodged and cracked SiC is entrapped between the sliding surfaces or incorporated into the soft aluminium matrix, resulting in extreme abrasion. The lack of the Al7075 matrix allowed the B_4C ceramic particles playing a more significant load-bearing role and increasing the potential of desquamation in the material. The desquamated B_4C and Al7075 matrix brought about changes in the wear behaviours and established abrasive wear as the predominate type of wear mechanism. The predominant wear mechanism of the Al7075 + SiC + B_4C composite shifted from abrasion wear to adhesion wear as the applied load became more severe. In the wear system comprising the pin and the disc, the shear stress desquamated the Al7075 matrix, resulting in the periodic plastic deformation of the B_4C/Al7075 composite. As shown in Fig. 19(c), the stress concentration was caused by the plastic deformation that occurred between the pin while the

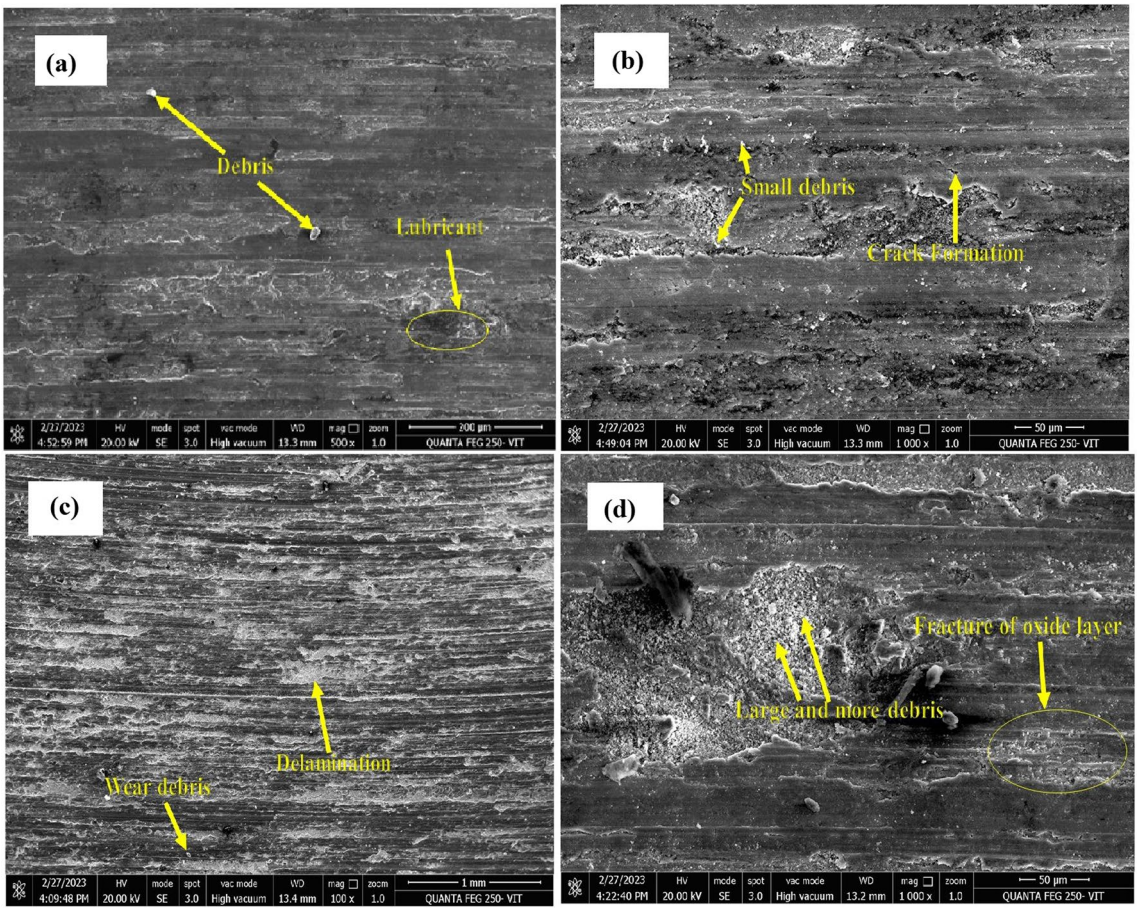

Fig. 19 FESEM image of composites worn surfaces **a** Al7075 + 4wt%SiC **b** Al7075 + 3wt%SiC **c** Al7075 + 6wt%SiC + 2wt%B_4C **d** Al7075 + 3wt%SiC + 2wt%B_4C

disc led to the delamination layer phenomenon of adhesion wear. This phenomenon protected the composite from further friction and enhanced the wear resistance of the Al7075 + SiC + B_4C composite [56].

3.11 Corrosion Analysis

3.11.1 Aluminium 7075 Alloy Reinforced SiC Composites

An electrochemical test was carried out using the Al7075 + SiC composites. The potentiodynamic experiments were carried out with 3.5% NaCl as electrolyte at room temperature. Before the samples were placed in the measuring vessel, they were cleaned and polished to a surface area of $1cm^2$. The composite sample as the working electrode, platinum as counter electrode, and saturated calomel as reference electrode. The Fig. 20(a) shows the Tafel plots for Al7075 with 2 to 6 wt% of SiC composites. The Ecorr and Icorr were determined by analysing the polarisation curves of the samples. The Icorr was obtained by extrapolating the anode and cathode polarisation curves using the Tafel plot. The anodic and cathodic regions of the TAFEL scan were used to acquire corrosion current density (Icorr) and potential voltage (Ecorr), betta cathodic (ßc), and betta anodic (ßa) slopes, as well as the corrosion rate, are shown in Table 6. The corrosion rate of the Al7075 + 6wt%SiC composites is generally superior to that of the Al7075 + 2wt%SiC and Al7075 + 4wt%SiC composites. Increasing the wt% of SiC particles will increase the corrosion rate of Al7075 composites. The well bonding between the reinforcement and the matrix makes the corrosion rate significantly decrease. The primary reason for the increase of corrosion resistance was, due to the uniform flow of reinforcements in the matrix. The fact that SiC ceramic particles stay inert in the NaCl solution may be the reason for Al7075 + 6wt%SiC composites' superior corrosion resistance, when compared with the Al7075 + 2wt%SiC and Al7075 + 4wt%SiC composites. The NaCl aqueous medium has less significant on the Al7075 composites. Moreover, with the addition of SiC particulates, the number of pits decreases in composite material. This is presumably because of the inadequate formation of the passive oxide layer caused by SiC particles that are dispersed throughout the Al matrix [57, 58]. This makes

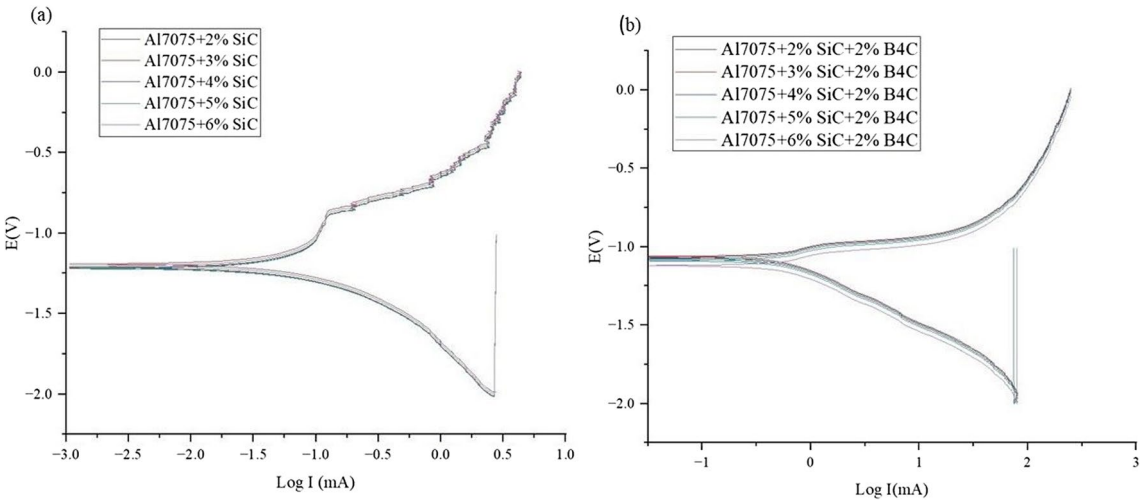

Fig. 20 **a** Polarisation curve of Aluminium 7075 reinforced with different wt% of SiC composites. **b** Polarisation curve of Aluminium 7075 reinforced with SiC and B_4C composites

the surface more electrochemically active, and as a result, Al7075 + 4wt%SiC corrodes at a quicker rate.

3.11.2 Aluminium 7075 Alloy Reinforced SiC and B_4C Composites

The Tafel plots of Al7075 + SiC + B_4C composites in 3.5% NaCl are represented in the Fig. 20(b). The corrosion current density (Icorr) and potential voltage (Ecorr), betta cathodic (ßc) and betta anodic (ßa) slopes, and the corrosion rate, are given in Table 7. The existence of hard ceramic reinforcement of SiC and B_4C particles in aluminium alloys matrix to improve the corrosion resistance. The results demonstrate that the composition of Al7075 + 2wt%SiC + 2wt%B_4C has a stronger corrosion resistance than all other aluminium 7075 composite samples. The improvement in corrosion resistance of composites can be attributed due to the electrochemical decoupling that most likely occurred between the B_4C particles and the Al7075 matrix. The rate of corrosion is increased in organic acid forms, and the polarisation curves are shifted to a region with a greater current density that is associated with neutral chloride forms. B_4C particles act as a physical defender, preventing the initiation of pitting corrosion and decreasing its rate of growth. The anodic polarization curve for Al7075 + SiC + B_4C shows the endurance in current corrosion density, which represents the exposure of pitting corrosion. The B_4C Particles, which are used as reinforcing components, prevent the formation of an oxide layer, which in turn increases the corrosion resistance of the composites. The corrosion rate of Al7075 + 5wt%SiC + 2wt%B_4C and Al7075 + 6wt%SiC + 2wt%B_4C hybrid metal matrix composites was greater than the corrosion rate of Al7075 + 2wt%SiC + 2wt%B_4C. In powder metallurgy components, corrosion can be caused by a combination of three factors: the pit, galvanic stress, and residual stress. This corrosion is caused by pits forming at the interfaces of the particles, residual stresses occurring during the compacting of the specimens during the process of manufacturing pellets, and galvanic corrosion occurring in between the particles. These are the factors that contribute to an enhanced rate of corrosion in the composites [59, 60].

Table 6 Ecorr, Icorr and corrosion rate measurements of Al7075 reinforced with different wt% of SiC composites

S.No	Sample Details	E_{corr} (mV)	I_{corr} (µA)	Cathodic Tafel Slope, ßc (mV)	Anodic Tafel Slope, ßa (mV)	Corrosion Rate (mpy)
1.	Al7075 + 2%SiC	-1026.032	0.477	197.8	142.1	0.230
2.	Al7075 + 3%SiC	-1129.942	0.340	230.1	155.1	0.170
3.	Al7075 + 4%SiC	-1238.978	1.488	290.1	234.8	0.758
4.	Al7075 + 5%SiC	-1067.633	0.329	249.8	69.0	0.169
5.	Al7075 + 6%SiC	-1131.376	0.324	178.1	108.5	0.167

Table 7 Ecorr, Icorr and corrosion rate measurements of Al7075 reinforced with different SiC and constant B_4C composites

S.No	Sample Details	E_{corr} (mV)	I_{corr} (μA)	Cathodic Tafel Slope, ßc (mV)	Anodic Tafel Slope, ßa (mV)	Corrosion Rate (mpy)
1.	Al7075 + 2%SiC + 2%B_4C	-1047.511	0.229	314.3	91.0	0.229
2.	Al7075 + 3%SiC + 2%B_4C	-1025.364	0.243	260.9	68.6	0.243
3.	Al7075 + 4%SiC + 2%B_4C	-1092.566	0.487	185.9	153.6	0.487
4.	Al7075 + 5%SiC + 2%B_4C	-1173.390	1.566	177.0	312.0	1.566
5.	Al7075 + 6%SiC + 2%B_4C	-1203.138	1.185	269.7	278.6	1.185

4 Conclusion

In this study, comparisons have been made between hybrid composites made of aluminium 7075 alloys, which were reinforced with varying amounts of SiC particles (2,3,4,5,6 wt%) and with the addition of a constant amount of 2 wt% B_4C particles and aluminium 7075 alloys, which were reinforced with SiC particles (2,3,4,5,6 wt%) of varying quantities. Powder metallurgy using the mechanical alloying technique was used in the manufacture of composites of both types of composites. An investigation of the mechanical properties of composites, including the impact of the reinforcements was made through analysis of the microstructure, hardness, XRD, density & porosity and reported.

- The microstructures of Al7075 + SiC reinforced composites were examined, and the results revealed the Al7075 + 5wt%SiC and Al7075 + 6wt%SiC composites making a consistent distribution of SiC particles in the Al matrix, while Al7075 + 2wt% SiC and Al7075 + 3wt%SiC composites were found with some agglomerations. The results of investigation using a scanning electron microscope showed the hybrid composite made of Al7075 + 3wt%SiC + 2wt%B_4C having a homogeneous structure and good interfacial bonding between the matrix and the reinforcement, whereas composites with Al7075 + 4wt%SiC + 2wt%B_4C and Al7075 + 6wt%SiC + 2wt%B_4C exhibited voids and agglomeration that increased as SiC reinforcement wt% was increased.
- The EBSD map determined that the grain size of the composites made of Al7075 + 6wt%SiC and Al7075 + 3wt%SiC + 2wt%B_4C was 2.3 μm and 19.6 μm, respectively.
- XRD analysis of Al7075 + SiC composites fabricated showed the aluminium (111) phase having a highest peak intensity, whereas the Al (222), and SiC (109) phases had low-intensity peaks. The XRD pattern indicated the presence of peaks for Aluminium, Zinc, SiC, and B_4C particles. The XRD analysis of Al7075 + SiC + B_4C composites revealed the Al (222) and Al (111) phases having the highest peak intensities. While the phases of Al (222) and B_4C (119) had low-intensity peaks.
- The composite made of Al7075 + 6 wt% SiC was found having a high hardness value of 195 HV. The increased hardness exhibited by the Al7075 + SiC composite was also due the uniform distribution of SiC throughout the composites produced. The addition of B_4C to Al7075 + 4wt%SiC + 2wt%B_4C and Al7075 + 5wt%SiC + 2wt%B_4C composites resulted in a drop in the hardness value of 112 HV and 139 HV, respectively. This was caused by a mismatch between the form and size of the reinforcement and the Al matrix.
- The composites Al7075 + 3%SiC and Al7075 + 4%SiC obtained improved compressive strength. The hybrid aluminium 7075 composites with the highest compression strength were Al7075 + 2wt%SiC + 2wt%B_4C and Al7075 + 3wt% SiC + 2wt% B_4C composites. The dispersion strengthening mechanism was seen as the most essential of all the strengthening processes that contribute to increase in the compressive strength of the composites.
- The limited number of pores in the sample caused high density in Al7075 + 2wt%SiC composite which helped achievement of a density value of 2.633 g/cm^3. The Al7075 + 3wt%SiC + 2wt%B_4C composite was found having a high-density value of 2.656 g/cm^3, whereas the Al7075 + 4wt%SiC + 2wt%B_4C composite was found to have a lower density value of 2.548 g/cm^3. The density test showed the presence of a weak bond between the B_4C phase and the Al 7075 phase, and the void percentage in the B_4C reinforced samples as larger than in the SiC reinforced samples.
- The hydrophobic surface was obtained for Al7075 + 6wt%SiC and Al7075 + 4wt%SiC + 2wt%B_4C hybrid aluminium 7075 alloy composites. Because the surface of aluminium 7075 composites had a water contact angle of 102.34°.
- It was found that the higher thermal conductivity of Al7075 + 6wt%SiC composite was obtained as 58.99 W/

mK. The higher thermal conductivity of Al7075 hybrid (2wt%SiC + 2wt%B_4C) composites was found to be 58.67 W/mK.

- The findings demonstrate that hybrid composites retaining their wear-resistant properties on 5N and 10 N and under the sliding speed of 0.1 m/s. The lowest wear rate was determined for Al7075 + 2wt%SiC and Al7075 + 4wt%SiC composites under the load of 5N and 10N respectively. The lowest wear rate of hybrid composites was determined for Al7075 + 4wt%SiC + 2wt%B_4C and Al7075 + 6wt%SiC + 2wt%B_4C composites under the load of 5N and 10N respectively.
- The addition of SiC and B_4C resulted in an increase in wear resistance, which could be due to the cooperating effect of the reinforcing particles. The increase in the percentage of SiC and B_4C particles in the Al7075 material results in a decrease in the material's coefficient of friction under the load of 5N.
- The wear mechanisms that occurred on the surfaces depended on the wear conditions and included abrasion and delamination. The wear mechanisms for aluminium 7075 composites could be determined through control over the wear conditions.
- The corrosion resistance was higher in Al7075 + 6wt%SiC composite and lesser in Al7075 + 2wt%SiC composite. The Al7075 + 2wt%SiC + 2wt%B_4C hybrid composites demonstrated a lower rate of corrosion compared to Al7075 + 6wt%SiC + 2wt%B_4C composite.

5 Applications

The objective of developing aluminium 7075 material as hybrid composites with the aid of various reinforcements is to improve the mechanical and wear properties, this is suggested for various automobile applications like bicycle frames, car bodies, car frames, gears, shafts, engine casings, engine mounts, fuse parts, worm gears, armoured vehicles, etc.

6 Future Scope of Work

The focus of future research, it is suggested, can be on conventional sintering processes, such as spark plasma sintering and microwave sintering, which could be utilised for improvement of the mechanical performance of hybrid composites. Additional research is necessary on the preparation techniques like Semisolid powder processing, Hot isostatic pressing, Diffusion bonding for the improvement of the overall performance of hybrid composites based on aluminium alloys, making them suitable for industrial and comprehensive use.

Acknowledgements The authors would like to thank VIT University for providing the facilities for this research.

Author Contributions P Bharathi: designed the concept, interpreted the data and wrote the manuscript; Dr.T Sampath Kumar: analysed and revised the manuscript.

Data Availability All data generated are analysed during this study are included in this published article.

Declarations

Ethics Approval Not applicable.

Consent to Participate Not applicable.

Consent for Publication The authors declare that the figures and tables used in this manuscript are original and are not published anywhere.

Competing Interests The authors declare no competing interests.

References

1. Srivyas PD, Charoo MS (2018) Role of Fabrication Route on the Mechanical and Tribological Behavior of Aluminum Metal Matrix Composites - A Review. Mater Today Proc 5:20054–20069. https://doi.org/10.1016/j.matpr.2018.06.372
2. Karabacak AH, Çanakçı A, Erdemir F et al (2022) Corrosion and Mechanical Properties of Novel AA2024 Matrix Hybrid Nanocomposites Reinforced with B_4C and SiC Particles. Silicon 14:8567–8579. https://doi.org/10.1007/s12633-021-01582-7
3. Singh KK, Singh S, Shrivastava AK (2017) Comparison of Wear and Friction Behaviour of Aluminium Matrix Alloy (Al 7075) and Silicon Carbide based Aluminium Metal Matrix Composite under Dry Condition at Different Sliding Distance. Mater Today Proc 4:8960–8970. https://doi.org/10.1016/j.matpr.2017.07.248
4. Bharathi P, Sampath kumar T (2022) Latest research and developments of ceramic reinforced magnesium matrix composites—A comprehensive review. Proc Inst Mech Eng E J Process Mech Eng. https://doi.org/10.1177/09544089221126044
5. Imran M, Khan ARA (2019) Characterization of Al-7075 metal matrix composites: A review. J Mater Res Technol 8:3347–3356. https://doi.org/10.1016/j.jmrt.2017.10.012
6. Garg P, Jamwal A, Kumar D et al (2019) Advance research progresses in aluminium matrix composites: manufacturing & applications. J Mater Res Technol 8:4924–4939. https://doi.org/10.1016/j.jmrt.2019.06.028
7. Dey D, Bhowmik A, Biswas (2022) A. Effect of SiC Content on Mechanical and Tribological Properties of Al2024-SiC Composites. Silicon 14:1–11. https://doi.org/10.1007/s12633-020-00757-y
8. Suhael Ahmed S, Girisha HN (2020) Experimental investigations on mechanical properties of Al7075/TiB_2/Gr hybrid composites. Mater Today Proc 46:6041–6044. https://doi.org/10.1016/j.matpr.2021.01.960
9. Manohar G, Pandey KM, Maity SR (2022) Effect of Variations in Microwave Processing Temperatures on Microstructural and Mechanical Properties of AA7075/SiC/Graphite Hybrid Composite Fabricated by Powder Metallurgy Techniques. Silicon 14:7831–7847. https://doi.org/10.1007/s12633-021-01554-x
10. Surya MS (2022) Effect of SiC Weight Percentage and Sintering Duration on Microstructural and Mechanical Behaviour of Al6061/SiC Composites Produced by Powder Metallurgy Technique. Silicon 14:2731–2739. https://doi.org/10.1007/s12633-021-01053-z

11. Manikandan R, Arjunan TV, Akhil AR (2020) Studies on micro structural characteristics, mechanical and tribological behaviours of boron carbide and cow dung ash reinforced aluminium (Al 7075) hybrid metal matrix composite. Compos Part B Eng 183. https://doi.org/10.1016/j.compositesb.2019.107668
12. Surya MS, Prasanthi G (2020) Manufacturing, microstructural and mechanical characterization of powder metallurgy processed Al7075/SiC metal matrix composite. Mater Today Proc 39:1175–1179. https://doi.org/10.1016/j.matpr.2020.03.315
13. Sattari S, Jahani M, Atrian A (2017) Effect of Volume Fraction of Reinforcement and Milling Time on Physical and Mechanical Properties of Al7075–SiC Composites Fabricated by Powder Metallurgy Method. Powder Metall Met Ceram 56:283–292. https://doi.org/10.1007/s11106-017-9896-2
14. Atrian A, Majzoobi GH, Enayati MH, Bakhtiari H (2014) Mechanical and microstructural characterization of Al7075/SiC nanocomposites fabricated by dynamic compaction. Int J Miner Metall Mater 21:295–303. https://doi.org/10.1007/s12613-014-0908-7
15. Halil K, Ismail OI, Sibel D, Çi R (2019) Wear and mechanical properties of Al6061/SiC/B_4C hybrid composites produced with powder metallurgy. J Mater Res Technol 8:5348–5361. https://doi.org/10.1016/j.jmrt.2019.09.002
16. Anil Kumar G, Sateesh J, Kumar TY, Madhusudhan T (2016) Properties of Al7075-B_4C Composite prepared by Powder Metallurgy Route. Int Res J Eng Technol 03:2395–2456
17. Tarakcioglu N, Canakci A, Varol T et al (2014) Enhanced properties of an AA7075 based metal matrix composite prepared using mechanical alloying. Usak Univ J Mater Sci 3:47–47. https://doi.org/10.12748/uujms.201416499
18. Zhao N, Nash P, Yang X (2005) The effect of mechanical alloying on SiC distribution and the properties of 6061 aluminium composite. J Mater Process Technol 170:586–592. https://doi.org/10.1016/j.jmatprotec.2005.06.037
19. Çanakçı A, Varol T (2012) Production and microstructure of AA2024-B_4C metal matrix composites by mechanical alloying method. Univ J Mater Sci 1:15–22
20. Ozkaya S, Canakci A (2016) Effect of the B4C content and the milling time on the synthesis, consolidation and mechanical properties of AlCuMg-B_4C nanocomposites synthesized by mechanical milling. Powder Techno 297:8–16. https://doi.org/10.1016/j.powtec.2016.04.004
21. Ramkumar KR, Sivasankaran S, Al-Mufadi FA et al (2019) Investigations on microstructure, mechanical, and tribological behaviour of AA 7075–x wt.% TiC composites for aerospace applications. Arch Civ Mech Eng 19:428–438. https://doi.org/10.1016/j.acme.2018.12.003
22. Kothiyal P, Joshi A, Mer KKS, Verma R (2021) The evaluation of microstructure, grain boundary character and micro texture of [Al/Si3N4/Al2O3] P nanocomposites fabricated through PM route and its influence on compressive and three-body wear properties. Mater Res Express 8:1–22. https://doi.org/10.1088/2053-1591/ac406b
23. Zeng X, Liu W, Xu B, et al (2018) Microstructure and mechanical properties of Al–SiC nanocomposites synthesized by surface-modified aluminium powder. Metals (Basel) 8:253. https://doi.org/10.3390/met8040253
24. Carneiro Í, Viana F, Vieira MF, et al (2019) EBSD analysis of metal matrix nanocomposite microstructure produced by powder metallurgy. Nanomaterials 9:878. https://doi.org/10.3390/nano9060878
25. Chand S, Chandrasekhar P, Roy S, Singh S (2021) Influence of Dispersoid Content on Compressibility, Sinterability and Mechanical Behaviour of B_4C/BN Reinforced Al6061 Metal Matrix Hybrid Composites Fabricated via Mechanical Alloying. Met Mater Int 27:4841–4853. https://doi.org/10.1007/s12540-020-00739-0
26. Soares E, Bouchonneau N, Alves E et al (2021) Microstructure and mechanical properties of AA7075 aluminium alloy fabricated by spark plasma sintering (SPS). Materials (Basel) 14:1–11. https://doi.org/10.3390/ma14020430
27. Sankhla AM, Patel KM, Makhesana MA et al (2022) Effect of mixing method and particle size on hardness and compressive strength of aluminium based metal matrix composite prepared through powder metallurgy route. J Mater Res Technol 18:282–292. https://doi.org/10.1016/j.jmrt.2022.02.094
28. Akbarpour MR, Alipour S, Azar FL, Torknik FS (2016) Microstructure and hardness of Al-SiC nanocomposite fabricated through powder metallurgy method. Indian J Sci Technol 9:1–12. https://doi.org/10.17485/ijst/2016/v9i42/101515
29. Fenghong C, Chang C, Zhenyu W et al (2019) Effects of Silicon Carbide and Tungsten Carbide in Aluminium Metal Matrix Composites. Silicon 11:2625–2632. https://doi.org/10.1007/s12633-018-0051-6
30. Varol T, Canakci A (2013) Effect of weight percentage and particle size of B_4C reinforcement on physical and mechanical properties of powder metallurgy Al2024-B_4C composites. Met Mater Int 19:1227–1234. https://doi.org/10.1007/s12540-013-6014-y
31. Muraliraja R, Arunachalam R, Al-Fori I et al (2019) Development of alumina reinforced aluminium metal matrix composite with enhanced compressive strength through squeeze casting process. Proc Inst Mech Eng Part L J Mater Des Appl 233:307–314. https://doi.org/10.1177/1464420718809516
32. Singh G, Goyal S (2018) Microstructure and mechanical behaviour of AA6082-T6/SiC/B_4C-based aluminium hybrid composites. Part Sci Technol 36:154–161. https://doi.org/10.1080/02726351.2016.1227410
33. Venkatesh VSS, Deoghare AB (2022) Microstructural Characterization and Mechanical Behaviour of SiC and Kaoline Reinforced Aluminium Metal Matrix Composites Fabricated Through Powder Metallurgy Technique. Silicon 14:3723–3737. https://doi.org/10.1007/s12633-021-01154-9
34. Zhang J, Shi H, Cai M et al (2009) The dynamic properties of SiCp/Al composites fabricated by spark plasma sintering with powders prepared by mechanical alloying process. Mater Sci Eng A 527:218–224. https://doi.org/10.1016/j.msea.2009.08.067
35. Shen Q, Wu C, Luo G, Fang P, Li C, Wang Y, Zhang L (2014) Microstructure and mechanical properties of Al-7075/B_4C composites fabricated by plasma activated sintering. J Alloys Compd 588:265–270. https://doi.org/10.1016/j.jallcom.2013.11.089
36. Kare D, Chintada S, Dora SP (2022) Damping Behavior of Al/SiC Composites Fabricated by Powder Metallurgy. Silicon 14:8255–8261. https://doi.org/10.1007/s12633-021-01497-3
37. Fogagnolo JB, Velasco F, Robert MH, Torralba JM (2003) Effect of mechanical alloying on the morphology, microstructure and properties of aluminium matrix composite powders. Mater Sci Eng A 342:131–143. https://doi.org/10.1016/S0921-5093(02)00246-0
38. Van Trinh P, Lee J, Minh PN et al (2018) Effect of oxidation of SiC particles on mechanical properties and wear behaviour of SiCp/Al6061 composites. J Alloys Compd 769:282–292. https://doi.org/10.1016/j.jallcom.2018.07.355
39. Zhang L, Shi J, Shen C et al (2017) B_4C-Al composites fabricated by the powder metallurgy process. Appl Sci 7:8–13. https://doi.org/10.3390/app7101009
40. Kumar N, Manoj MK (2021) Influence of B_4C on Dry Sliding Wear Behaviour of B_4C/Al–Mg–Si Composites Synthesized via Powder Metallurgy Route. Met Mater Int 27:4120–4131. https://doi.org/10.1007/s12540-020-00814
41. Singh VK, Chauhan S, Gope PC, Chaudhary AK (2015) Enhancement of Wettability of Aluminum Based Silicon Carbide Reinforced Particulate Metal Matrix Composite. High Temp Mater Process 34:163–170. https://doi.org/10.1515/htmp-2014-0043
42. An Q, Cong XS, Shen P, Jiang QC (2019) Roles of alloying elements in wetting of SiC by Al. J Alloys Compd 784:1212–1220. https://doi.org/10.1016/j.jallcom.2019.01.138

43. Sharma VK, Kumar V, Joshi RS (2020) Parametric study of aluminium-rare earth based composites with improved hydrophobicity using response surface method. J Mater Res Technol 9:4919–4932. https://doi.org/10.1016/j.jmrt.2020.03.011
44. Hashim J, Looney L, Hashmi MSJ (2001) The wettability of SiC particles by molten aluminium alloy. J Mater Process Technol 119:324–328. https://doi.org/10.1016/S0924-0136(01)00975-X
45. Sharifi H, Eidivandi V, Tayebi M et al (2017) Effect of SiC particles on thermal conductivity of Al-4%Cu/SiC composites. Heat Mass Transf 53:3621–3627. https://doi.org/10.1007/s00231-017-2073-9
46. Zare R, Sharifi H, Saeri MR, Tayebi M (2019) Investigating the effect of SiC particles on the physical and thermal properties of Al6061/SiCp composite. J Alloys Compd 801:520–528. https://doi.org/10.1016/j.jallcom.2019.05.317
47. Almadhoni K, Khan S (2015) Evaluation of the Effective Thermal Properties of Aluminum Metal Matrix Composites Reinforced by Ceramic Particles. Int J Curr Eng Technol 5:2884–2897
48. Devaiah M (2018) Comparison of Thermal Conductivity Experimental Results of SIC P /AL 2 O 3 Ceramic Matrix Composites with Mathematical Modeling. Int J Appl Eng Res 13:3784–3788
49. Bhowmik A, Dey S, Dey D et al (2021) Dry Sliding Wear Performance of Al7075/SiC Composites by Applying Grey-Fuzzy Approach. SILICON 13:3665–3680. https://doi.org/10.1007/s12633-020-00930-3
50. Gupta P, Kumar D, Parkash O et al (2018) Dependence of wear behaviour on sintering mechanism for Iron-Alumina Metal Matrix Nanocomposites. Mater Chem Phys 220:441–448. https://doi.org/10.1016/j.matchemphys.2018.08.079
51. Kumar GBV, Rao CSP, Selvaraj N (2012) Mechanical and dry sliding wear behaviour of Al7075 alloy reinforced with SiC particles. J Compos Mater 46:1201–1209. https://doi.org/10.1177/0021998311414948
52. Sharif EM, Karimzadeh F (2011) Wear behaviour of aluminium matrix hybrid nanocomposites fabricated by powder metallurgy. Wear 271:1072–1079. https://doi.org/10.1016/j.wear.2011.05.015
53. Bharathi P, Kumar TS (2023) Mechanical Characteristics and Wear Behaviour of Al/SiC and Al/SiC/B_4C Hybrid Metal Matrix Composites Fabricated Through Powder Metallurgy Route. Silicon. https://doi.org/10.1007/s12633-023-02347-0
54. Nagaral M, Deshapande RG, Auradi V (2021) Mechanical and Wear Characterization of Ceramic Boron Carbide-Reinforced Al2024 Alloy Metal Composites. J Bio Tribo Corros 7:19. https://doi.org/10.1007/s40735-020-00454-8
55. Uthayakumar M, Aravindan S, Rajkumar K (2013) Wear performance of Al-SiC-B_4C hybrid composites under dry sliding conditions. Mater Des 47:456–464. https://doi.org/10.1016/j.matdes.2012,11(0),pp.51
56. Tang Feng Wu, Xiaoling GS, Jichun Ye, Hua Z, Masuo H (2008) Dry sliding friction and wear properties of B_4C particulate – reinforced Al-5083 matrix composites. Wear 264:555–561
57. Zakaria HM (2014) Microstructural and corrosion behavior of Al/SiC metal matrix composites. Ain Shams Eng J 5:831–838. https://doi.org/10.1016/j.asej.2014.03.003
58. Mahdi SM, Ghalib L (2022) Corrosion Behavior of Al/SiC Composite Prepared by Powder Metallurgy in Chloride Environments. J Bio- Tribo-Corrosion 8:1–11. https://doi.org/10.1007/s40735-021-00612-6
59. Meignanamoorthy M, Ravichandran M, Mohanavel V et al (2021) Microstructure, mechanical properties, and corrosion behavior of boron carbide reinforced aluminum alloy (Al-fe-si-zn-cu) matrix composites produced via powder metallurgy route. Materials (Basel) 14:431. https://doi.org/10.3390/ma14154315
60. Kumar KSR, Poornima CL (2016) Evaluation of Mechanical behaviour of Powder Metallurgy-Processed Aluminium Self Lubricating Hybrid Composites with B_4C Gr Additions. IJRMET 5762:120–127